Check for updates

RESEARCH ARTICLE

REVISED Identifying the performance and losses of a scroll compressor with vapour injection and R1234ze(E)

[version 2; peer review: 2 approved]

George Meramveliotakis[1,2], George Kosmadakis[1], Sotirios Karellas[2]

[1]Thermal Hydraulics and Multiphase Flow Laboratory, National Center for Scientific Research Demokritos, Agia Paraskevi, 15341, Greece
[2]Laboratory of Steam Boilers and Thermal Plants, National Technical University of Athens, Athens, 15780, Greece

v2 **First published:** 20 Apr 2022, **2**:49
https://doi.org/10.12688/openreseurope.14658.1
Latest published: 28 Nov 2022, **2**:49
https://doi.org/10.12688/openreseurope.14658.2

Abstract

This work investigates a vapour injection scroll compressor integrated in a heat pump using the refrigerant R1234ze(E). The water-to-water heat pump was tested under a wide temperature range at the evaporator and condenser sides. The test results revealed that the performance is significantly reduced for lifts of over 30 K with the coefficient of performance being even below 2 and the maximum 2nd law efficiency was just 28%. In order to enlighten the reasons behind such significant compressor underperformance, a semi-empirical model has been extended to include vapour injection, and a new improved modelling approach for the suction pressure drop was developed and implemented considering both the turbulent and laminar inlet flow regimes. Once the accuracy of the developed semi-empirical model was verified, the model was then adjusted to account for the R1234ze(E) operation, by fine-tuning its parameters based on the test data. The main loss mechanism identified is the high suction pressure drop, due to the high friction factor, with the inlet refrigerant flow possibly being laminar instead of turbulent. This resulted in a significant reduction of the mass flow rate and volumetric efficiency, while the standard model for suction pressure drop was not able to capture this effect.

Keywords

scroll compressor, HFO refrigerant, R1234ze(E), semi-empirical model, suction pressure drop, vapour injection, heat pump

H2020 This article is included in the Horizon 2020 gateway.

Open Peer Review

Approval Status ✓ ✓

	1	2
version 2 (revision) 28 Nov 2022		✓ view
version 1 20 Apr 2022	✓ view	? view

1. **Nicolas Tauveron**, Grenoble Alpes University, Le Bourget du Lac, France

2. **Christoph Wieland**, Technical University of Munich, Garching, Germany

Any reports and responses or comments on the article can be found at the end of the article.

Corresponding author: George Kosmadakis (gkosmad@ipta.demokritos.gr)

Author roles: Meramveliotakis G: Conceptualization, Formal Analysis, Investigation, Methodology, Software, Writing – Original Draft Preparation; **Kosmadakis G**: Conceptualization, Formal Analysis, Investigation, Methodology, Supervision, Writing – Review & Editing; **Karellas S**: Investigation, Supervision, Writing – Review & Editing

Competing interests: No competing interests were disclosed.

Grant information: This work has been implemented within the Renewables for clean energy buildings in a future power system (RES4BUILD) project that has received funding from the European Climate, Infrastructure and Environment Executive Agency (CINEA) under the European Union's Horizon 2020 research and innovation programme (grant agreement No 814865).
The funders had no role in study design, data collection and analysis, decision to publish, or preparation of the manuscript.

Copyright: © 2022 Meramveliotakis G *et al*. This is an open access article distributed under the terms of the Creative Commons Attribution License, which permits unrestricted use, distribution, and reproduction in any medium, provided the original work is properly cited.

How to cite this article: Meramveliotakis G, Kosmadakis G and Karellas S. **Identifying the performance and losses of a scroll compressor with vapour injection and R1234ze(E) [version 2; peer review: 2 approved]** Open Research Europe 2022, **2**:49 https://doi.org/10.12688/openreseurope.14658.2

First published: 20 Apr 2022, **2**:49 https://doi.org/10.12688/openreseurope.14658.1

REVISED **Amendments from Version 1**

The manuscript has been revised according to the comments and suggestions of both reviewers. Minor typos have been corrected and the quality of the figures improved, while the main changes to the text are highlighted next:

- A new section has been added that compares the two refrigerants R407C and R1234ze(E), including a new table (Table 3) and a new figure (Figure 4).
- The introduction section has been enriched mostly regarding low-GWP refrigerants, high-temperature heat pumps and oil performance with the addition of new references.
- Further details of the developed model (e.g. compressor electrical power) and the fitted friction factor correlation have been added in the model description section.
- The description of the testing facilities and of the heat pump has been enriched, by also providing some details of the two expansion valves.
- The refrigerant cycle in a pressure-enthalpy chart has been added (new Figure 6).
- In the test conditions paragraph, comments have been included for the system operating conditions and the data set selection.
- In the Data reduction part, additional information for the data processing (cycle analysis) have been added (Table 6–Table 7 revised).
- In the discussion of the results, Figure 8, Figure 9 and Figure 10 were modified to also contain the performance with R407C (with additional comments).

Any further responses from the reviewers can be found at the end of the article

Introduction

Hydrofluorocarbon (HFC) refrigerants are widely used in heat pumps and refrigeration systems. Although many of those have zero ozone depletion potential (ODP), their contribution to the global warming effect is still significant. According to the EU F-Gas regulation[1] and Kigali amendment to the Montreal Protocol[2], the use of HFCs is to be reduced, gradually moving towards their phase out due to the imposed strict limitations regarding their global warming potential (GWP). The most common HFCs such as R134a, R407C and R410A have a GWP of over 1400[3] and will need to be replaced by refrigerants that combine both low GWP and acceptable performance in heat pump systems. For this purpose, many alternatives are examined and evaluated focusing on low GWP refrigerants preferably with a GWP less than 150[1]. Several refrigerants have been proposed such as natural refrigerants (ammonia and CO_2), hydrocarbons (HCs), hydrofluoroolefins (HFOs), hydrochlorofluoroolefins (HCFOs) and mixtures of these substances[4].

HFOs are characterized by very low GWP (GWP<10), zero ODP, low or no flammability, non-toxicity[5] and can be considered as promising HFC replacements. The most widely used HFO is R1234yf, charged in many automotive air conditioning systems as a replacement of R134a[6]. Another alternative to R134a for medium temperature applications is R1234ze(E)[5,7] with a GWP equal to 4, which is applied as a pure substance or a mixture component in many applications[8]. To evaluate its potential, Babiloni *et al.*[9] tested a vapour compression system with an internal heat exchanger (IHX) operating with R1234yf and R1234ze(E). Their results showed that the volumetric efficiency with both HFOs reduced by 3% to 6% compared with R134a, leading to a cooling capacity decrease of 9% and 30% respectively. In terms of performance, the coefficient of performance (COP) of R1234yf was 3 to 11% lower than that of R134a, with a similar reduction for R1234ze(E) (2% to 8%). Another study by Jankovic *et al.*[10] performed both experimental and numerical evaluation of R1234yf and R1234ze(E) as R134a replacements in a refrigeration system. Their overall conclusions are similar as the ones of Reference 9, since the cooling capacity was reduced by 6% and 27% with R1234yf and R1234ze(E) respectively, while the COP decrease was below 5% for both HFOs. In general, R1234yf was proposed as a more suitable replacement for low to medium temperature heat pumps, while R1234ze(E) for higher temperature purposes[11].

Mendoza *et al.*[12] extended the refrigerant range of R134a alternatives, by also investigating the HFO blend R450A, as well as R1234yf and R1234ze(E) in a reciprocating compressor. Their tests were conducted over a wide range of operating conditions, and they developed a model based on dimensionless numbers, in order to examine their performance. Higher volumetric and isentropic efficiencies were observed for R450A compared with the other alternative refrigerants, but still lower than those seen in R134a by about 5-6%. Moreover, R1234ze(E) had the lowest cooling capacity, but its COP was slightly lower than the one of R134a and higher than R1234yf and R450A.

It becomes clear that the main deficit of HFOs is the lower capacity. To overcome this, especially at high temperature lifts, vapour injection has been proposed that finds application in scroll and screw compressors[13]. The main advantage of this technique is the rise of the capacity by controlling the injected refrigerant mass flow rate[14]. Furthermore, it provides cooling to the compressor, decreasing the discharge temperature[15] and therefore, the operating envelope of the compressor can be expanded, compared to the standard vapour compression cycle. Additionally, the injection technique, especially with liquid refrigerant, decreases the oil temperature leading to better oil performance and reduces oil degradation effects[16]. Lumkin *et al.*[17] generated dimensionless correlations to map the compressor performance based on the Buckingham-PI method using experimental data of a R407C scroll compressor with vapour and liquid-vapour injection. Also, the proposed correlations, were validated using data points from a variable-speed R410A vapour injection scroll compressor providing very high accuracy especially for predicting the injection ratio and compressor power.

Winandy and Lebrun[18], Cho *et al.*[19] and Wang *et al.*[20] have investigated the effect of vapour injection on heat pump systems with scroll compressors using HFCs, showing encouraging test results for heating capacity and COP. In the case of

HFOs, Shuxue *et al.*[21] examined the performance of a vapour injected scroll compressor in a heat pump configuration with R1234yf and a R1234yf/R32 mixture and tested for low ambient temperatures. The heating capacity was improved due to the increase of the compressor discharge mass flow from 5% to 20% compared to the non-injected case. Shuxue and Guoyuan[22] performed similar tests on a vapour injection scroll compressor but with R1234ze(E) and a R32/R1234ze(E) mixture for electric vehicles air conditioning. The evaporating temperatures were low, and the operation with R1234ze(E) and vapour injection extended the minimum temperature limit to below -20 °C, and at the same time significantly increasing the heating capacity and the COP compared with the system without vapour injection.

Additionally to the experimental investigations of compressors with vapour injection, several relevant numerical studies have been also carried out. Fukuda *et al.*[23] evaluated R1234ze(E) and R1234ze(Z) as alternative fluids for high temperature heat pumps (HTHPs) which are classified based on the output temperature in the range between 100 – 160 °C[4]. The main results revealed major inadequacies between theoretical and experimental findings, mostly related to the COP values, due to significant reduction of the volumetric capacity caused by irreversible losses. Further analysis of the losses showed that R1234ze(Z) provided better performance at high temperatures, as also concluded in Reference 24, because the losses related to the pressure drop were significantly reduced. For that reason, these two refrigerants were proposed as suitable ones for HTHPs. Regarding other numerical models, Wang *et al.*[25] developed a geometrical model for a scroll compressor with vapour injection operating with R22. Based on simulations and experiments, the refrigerant injection was modelled as a parameter-varying process described by adiabatic throttling of the injected refrigerant up to the pressure inside the scroll pocket, with a simultaneous isobaric mixing of the two streams. Another geometrical model was developed in Reference 26 for a variable speed scroll compressor by using continuity, energy conservation and real gas equations. The model was validated with R22 and the injection conditions as well as the port geometry were analyzed based on the rotational frequency.

Due to the high complexity and computational cost of the geometrical models, semi-empirical models have also been developed to describe the several processes within the compressor. Winandy and Lebrun[18] developed such model for both vapour and liquid injection with its parameters fine-tuned for R22. The injection was assumed to be carried out after the closure of the suction pocket while leakages and pressure drops were not considered. The prediction accuracy was within ±4%, ±4.5%, and ±5 K for the mass flow rate, compressor power and discharge temperature of the compressor respectively. Another semi-empirical model was developed by Dardenne *et al.*[27] for a variable speed scroll compressor with R410A. The vapour injection is described by decomposing the process into several steps during the isentropic part of the compression. The injection flow in the compressor is not considered constant,[28], but rather it varies according to the pressure difference between the injection line and the compressor pocket. The semi-empirical model also includes compressor leakages, resulting in a set of 10 parameters that need to be fine-tuned with experimental data. A different approach has been followed by Tello-Oquendo *et al.*[29], who used a linear correlation of the injected mass flow as a function of the intermediate pressure and the given suction conditions. The model takes into consideration the main sources of losses such as the suction and discharge pressure drop and the compressor leakages. For the model validation, different non-injected scroll compressors were tested with R290 and a vapour injection scroll compressor with R407C. Their results revealed that for the latter the isentropic and volumetric efficiency was predicted with a deviation lower than ±5% compared with the experimental data.

Overall, the low GWP HFO refrigerants, such as R1234yf and R1234ze(E), provide a decreased performance and capacity, when they are used as drop-in alternatives. In order to combat this effect, vapour injection has been proposed in scroll compressors as a promising way to enhance the system capacity. But still the loss mechanisms are not well defined compared with the ones using the standard HFC refrigerants, with the relevant experimental facilities aiming mostly to identify the overall performance and capacity. The current work aims to cover this gap, by following a combined experimental and numerical approach. Once the semi-empirical model is developed with advanced features, including a more precise model for the suction pressure drop, and fine-tuned with the use of the test data, it is then applied to provide a better understanding of the compressor losses with the final objective to locate the reasons for low heat pump performance and 2nd law efficiency.

Improving the semi-empirical model

The semi-empirical model has been verified in Reference 29 for different scroll compressors (without vapour injection) operating with a variety of HFC and HFO refrigerants relying on the initial methodology proposed by Winandy *et al.*[30]. The model is further extended here to describe vapour injection, in order to evaluate the prediction accuracy and compressor performance based on experimental results with R1234ze(E) refrigerant. At the same time, a new numerical approach for modeling the suction pressure drop has been developed, considering both laminar and turbulent flow at the suction line, aiming to further improve the prediction accuracy, even at conditions outside the operating envelope of the compressor.

Semi-empirical model of a scroll compressor with vapour injection

The model introduces one injection line at the compressor and splits the compression into two stages. The first one refers to the isentropic compression from the suction conditions to the intermediate state, while the second one considers the refrigerant after the adiabatic mixing up to the adapted conditions (identified by the built-in volume ratio). The intermediate state is where the vapour is injected, and its properties are identified via corresponding pressure, temperature, and mass flow rate. The refrigerant properties are identified through the built-in thermodynamic libraries available

in the Engineering Equation Solver (EES) software[31]. As an open-source alternative, many thermodynamic libraries are also available and can be adapted in programing languages like Python. The complete evolution of the refrigerant in the compressor with the different processes that take place are described next.

1. Isobaric heating-up of the supply (su→su1), due to the hot motor and the casing. This process is related to the operating pressure ratio[32] and affects the actual trapped volume of the refrigerant, having a major impact on the volumetric efficiency of the compressor.

2. Adiabatic pressure drop at the suction port (su1→su2) which further influences the inlet conditions, by reducing the refrigerant pressure and density. Once this pressure drop increases, less refrigerant mass enters the compression chamber, leading to a reduction of the volumetric efficiency and as a result, of the overall performance.

3. Adiabatic mixing of supply flow with the leakage flow (su2→su3) due to the clearances between the bottom and top plate as well as the sidewalls of the scrolls.

4. Isentropic compression of the primary suction mass flow up to the intermediate pressure (su3→int), in which the vapour injection takes place. The intermediate state is identified by assuming the same absolute pressure between the injection suction line and the position inside the compressor after the injection port.

5. Isobaric mixing of the compressed suction mass flow with the injected vapour (int→int1).

6. Isentropic compression of the mixed flow up to the adapted conditions (int1→ad) which correspond to the built-in volume ratio of the compressor.

7. Adiabatic compression at constant volume due to the opening of the discharge valve from the adapted state up to the exhaust pressure (ad→ex1).

8. Leaking flow to the compressor inlet (ex1→ex1.1) due to the pressure difference that pushes out refrigerant from the clearances. The internal leakages are modelled assuming isentropic flow through a convergent nozzle with a cross-sectional area of the throat equal to the total leakage area of the compressor.

9. Isobaric cooling down at a constant wall temperature of T_w (ex1→ex2) due to the heat transfer between the high-temperature discharge refrigerant and the compressor casing. A part of this heat is lost to the ambient through the casing.

10. Adiabatic pressure drop at the exhaust port to the final discharge pressure (ex2→ex). This pressure loss is modelled assuming isentropic flow in a converging nozzle followed by an isobaric diffuser.

The compressor sub-processes including vapour injection and the corresponding pressure-enthalpy diagram are shown in Figure 1, with the supply side highlighted in blue, the compression with black and the exhaust with red colored lines. Further details of each sub-process along with their mathematical formulation are found in Reference 29.

The input data are the compressor supply temperature (T_{su}), the evaporating and condensing pressures (P_{su} and P_{ex}), the ambient temperature (T_{amb}), the compressor speed (N_{cp}), and the ones related to the vapour injection: the intermediate pressure and temperature (P_{int} and T_{int}) and the injected mass flow rate ($\dot{m}_{vi}$).

The sub-processes highlighted above introduced a set of 12 parameters in total, that are fine-tuned with the use of available

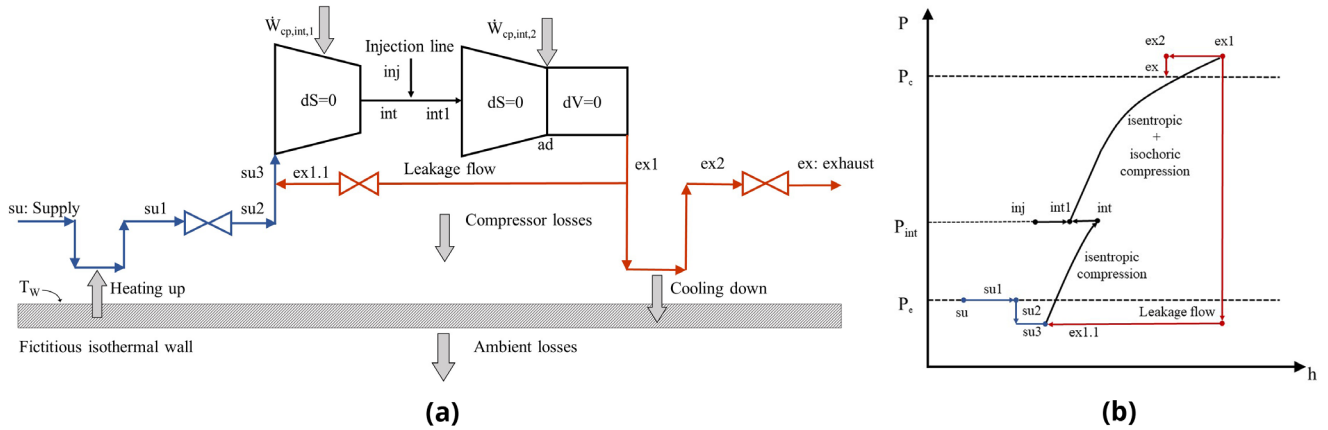


Figure 1. Compressor sub-processes with vapour injection (su1: supply after heating up; su2: supply after heating up and pressure drop; su3: inlet to compressor; dS=0: isentropic; -pcp,int,1: power of 1st stage compression; int: outlet of 1st compression stage; inj: injection; int1: inlet to 2nd compression stage; etcp,int,2: power of 2nd stage compression; ad: adiabatic; dV=0: isochoric; ex1: outlet of 2nd compression stage; ex2: outlet after cooling down): (**a**) schematic diagram highlighting the different states; (**b**) generic pressure-enthalpy chart.

data from either the free software of the compressor manufacturer or experimental results, as discussed later in this work. This is achieved once minimizing the defined function Θ (Equation. (1)) by implementing a genetic algorithm optimization process[33].

$$\Theta = \sqrt{\frac{1}{Z}\sum_{i=1}^{Z}\left[\left(\frac{T_{calc,i} - T_{data,i}}{T_{data,i}}\right)^2 + \left(\frac{\dot{m}_{calc,i} - \dot{m}_{data,i}}{\dot{m}_{data,i}}\right)^2 + \left(\frac{\dot{W}_{calc,i} - \dot{W}_{data,i}}{\dot{W}_{data,i}}\right)^2\right]} \quad (1)$$

Where Z is the total number of datasets, subscripts *calc* and *data* correspond to the calculated values and the available data and T, $\dot{m}$ and $\dot{W}$ refer to the discharge temperature, mass flow rate and electric power respectively.

The basic compressor model algorithm is depicted in Figure 2 and was developed under the EES environment[31] due to the flexibility of thermodynamic properties calculations and built-in optimization tools, selecting the genetic algorithms for this work to reach the global optimum.

The set of the model parameters is shown in Table 1. The parameters D_{ex} and corr are identified according to technical specifications given by the compressor manufacturer and the literature respectively, while $\dot{m}_{r,cp,n}$ is the reference mass flow rate calculated from the nominal swept volume multiplied by the density for a saturated vapour at 0 °C. The other nine parameters are identified by the function Θ minimization.

In order to model the whole vapor injection process, two more equations are needed related to steps 4, 5 and 6 presented previously. The isobaric mixing between the injection flow

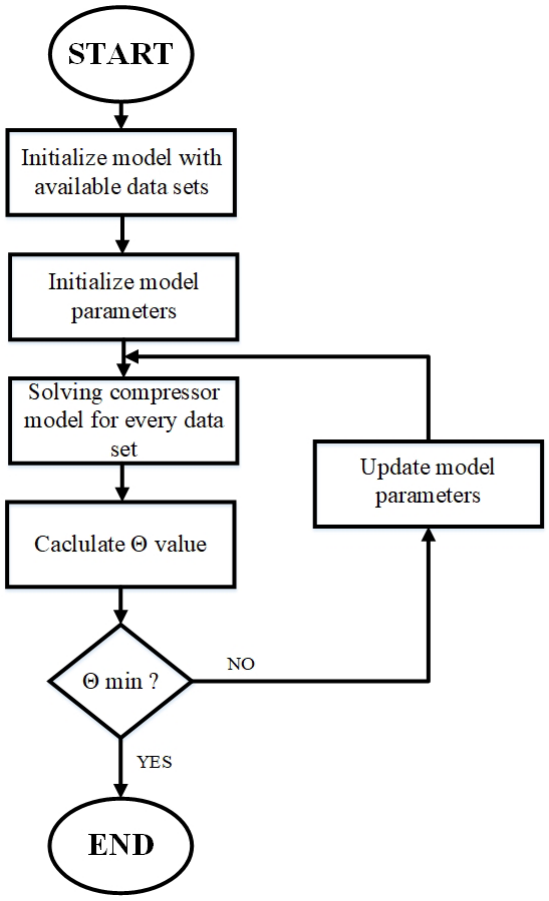


Figure 2. Flowchart of the compressor model.

Table 1. Parameters of the semi-empirical model and relevant compressor sub-processes with vapour injection.

Parameter	Units	Sub-process
$AU_{su,cp,n}$	W/K	Heat transfer coefficient for heating-up during supply
$AU_{ex,cp,n}$	W/K	Heat transfer coefficient for heat loss during the exhaust
AU_{amb}	W/K	Heat transfer coefficient for heat losses to the ambient
A_{leak}	m^2	Effective area of leakages
$\dot{W}_{cp,loss,0}$	W	Constant term of the electrical power losses
a_{cp}	-	Coefficient of the variable term of the electrical power losses
D_{ex}	m	Exhaust diameter for discharge pressure losses
corr	1/W	Motor slip coefficient
$r_{v,in}$	-	Built-in volume ratio of the compression process
$\dot{m}_{r,cp,n}$	kg/s	Nominal mass flow of the refrigerant
$V_{s,cp}$	m^3	Swept volume of the compressor
K	$1/m^4$	Lumped friction factor parameter

and the compressed mass inside the scrolls are described by Equation. (2) and Equation. (3) respectively.

$$\dot{m}_{vi} h_{r,inj} + \dot{m}_{r,cp,su3} h_{r,int} = \dot{m}_{r,cp} h_{r,int1} \quad (2)$$

$$\dot{m}_{r,cp} = \dot{m}_{vi} + \dot{m}_{r,cp,su3} \quad (3)$$

$$R_{vi} = \frac{\dot{m}_{vi}}{\dot{m}_{r,cp,su3}} \quad (4)$$

Where $\dot{m}_{vi}$ is the injected mass flow rate, $\dot{m}_{r,cp,su3}$ is the mass flow rate after the first compression stage, $\dot{m}_{r,cp}$ is the compressor mass flow after mixing, $h_{r,inj}$ is the refrigerant enthalpy at the injection line, $h_{r,int}$ is the refrigerant enthalpy at the intermediate state inside the compressor, $h_{r,int1}$ is the enthalpy after the mixing of the two streams, and R_{vi} is the ratio between the injected and suction mass flow rates.

Due to the splitting of the whole compression into two stages, the calculation of the compression work requires an additional term. The total internal work provided to the compressor (w_{in}) is then given by Equation. (5).

$$w_{in} = w_{in1,is} + w_{in2,is} + w_{in,v} = (h_{r,int} - h_{r,su3}) + (h_{r,ad} - h_{r,int1}) + v_{r,ad}(P_{ex1} - P_{ad}) \quad (5)$$

Where $w_{in1,is}$ and $w_{in2,is}$ is the required work for the isentropic compression from the initial (su3) to the intermediate (int) and from the intermediate to the built-in (ad) volume respectively, the subscript r refers to the refrigerant side and the int1 represents the thermodynamic state obtained after the isobaric mixing with the vapour injection line. Also, $w_{in,v}$ is the work corresponding to the constant volume part and is obtained by the constant specific volume calculated in the adapted conditions ($v_{r,in}$) multiplied by the pressure difference of the exhaust (P_{ex1}) with the adapted (P_{ad}) state.

The main performance indicators of the compressor are the volumetric and isentropic efficiency determined by Equation. (6)–Equation. (7). The volumetric efficiency (η_{vol}) is defined as the ratio of the actual mass flow that enters the compressor to the theoretical one, calculated at the suction position by using the nominal volumetric flow rate[34]. The isentropic efficiency (η_{is}) expresses the ratio of the ideal to the actual power consumption, adjusted for vapour injection compressors, as proposed in References 17,35 according to ASHRAE (American Society of Heating, Refrigerating and Air-Conditioning Engineers) standard 23.1[36].

$$n_{vol} = \frac{\dot{m}_{r,cp,su3}}{\rho_{su} \dot{V}_{cp}} \quad (6)$$

$$\eta_{is} = \frac{\dot{m}_{r,cp,su3}(h_{r,int,is} - h_{r,su3}) + \dot{m}_{r,cp}(h_{r,ex,is} - h_{int1})}{\dot{W}_{cp}} \quad (7)$$

Where ρ_{su} is the density at the compressor suction, $\dot{V}_{cp}$ is the volumetric flow rate calculated by the nominal swept volume and the rotational speed[37], $h_{r,int,is}$ is the outlet enthalpy once the refrigerant is compressed isentropically from the suction up to the intermediate state, $h_{r,ex,is}$ refers to the specific enthalpy of the fluid following an isentropic compression from the intermediate state after mixing with injection line up to the discharge, and $\dot{W}_{cp}$ is the total electrical power provided to the compressor that includes the electromechanical conversion and all related losses.

Development of an improved suction pressure drop model

The numerical model of the suction pressure drop that has been previously included in the compressor model is the one proposed by Tello-Oquendo *et al.*[29]. This is based on the Darcy-Weisbach equation introducing a non-dimensionless friction factor that includes all the geometric characteristics that affect pressure drop (Equation. (8)).

$$\Delta P_{suc} = f \cdot \rho_{su} \cdot \frac{u^2}{2} = f \cdot \rho_{su} \cdot \frac{(n_{vol} \dot{V}_s)^2}{2 \cdot A_{su}^2} = K \cdot \frac{\rho_{su}}{2} \cdot (n_{vol} \dot{V}_{cp})^2 \quad (8)$$

Where f is the Darcy-Weisbach friction factor, u is the inlet velocity, A_{su} is the effective area of the suction port, and K is the lumped friction factor parameter that includes all the geometric features.

When the compressor operates within its envelope, the flow at the suction is typically a fully developed turbulent one, resulting to an almost constant friction factor according to the Moody chart[38]. However, when the compressor operation exceeds the envelope limits or the properties of the working fluid differ from the ones of the compressor's compatible refrigerants, the fluid flow may not remain turbulent. In the case of a low refrigerant suction pressure and density, the flow velocity is reduced, possibly reaching the laminar regime, in which the friction losses are proportional to the velocity. The outcome is a strong variation of the friction factor with a Reynolds number that needs to be modelled with a suitable correlation.

Such correlation has been developed in this study, by initially examining the effect of the flow regime on the friction factor. In the case of a laminar flow (with $Re<2300$) the Hagen-Poiseuille equation[39] (Equation. (9)) applies.

$$f = \frac{64}{Re} \quad (9)$$

Where Re is the Reynolds number of the working fluid.

For a transient or turbulent flow ($Re>2300$), the friction factor is commonly described by the Colebrook-White equation[40] (Equation. (10)).

$$f = -2 \log_{10}\left(\frac{2.51}{Re\sqrt{f}} + \frac{\varepsilon}{3.71D}\right) \quad (10)$$

Where ε/D is the relative roughness of the inner surface of the inlet pipe, with its range of practical interest between 10^{-6} and 0.05.

Several correlations have been developed that provide the friction factor over an extended Reynolds number range with a good accuracy[39]. Some common ones for both laminar and

turbulent regimes and all relative roughness ranges are given in Table 2. These expressions are implicit functions including the relative roughness and the *Re*.

With the aim to expand the validity of the calculations over the whole range of the Reynolds number, and at the same time to avoid the estimation of the unknown geometric characteristics, a logarithmic expression is developed as a function of only the Reynolds number, instead of using an implicit equation from the available ones. The necessity of a new equation is based on the fact that the $\frac{\varepsilon}{D}$ ratio at the compressor inlet is an unknown parameter. For that reason, all the geometrical parameters that impact on the friction factor are lumped in the calibration parameters A_0 and A_1 of Equation. (11).

$$f(Re) = A_0 + A_1[\log_{10}(Re)]^{-3} \quad (11)$$

This type has been preferred due to the logarithmic relation between friction factor and Reynolds number as shown in the relevant literature[39]. This equation involves two parameters that need to be calibrated, in order for its results to match with the ones of Table 2 for every $\frac{\varepsilon}{D}$ value. The inverse cubed exponent in Equation. (10) is chosen by a best-fit procedure, in order for the correlation to closely follow the results of the

Table 2. Literature correlations for Darcy-Weisbach friction factor calculation.

Correlations	Reference
$f = 5.5 \cdot 10^3 \left[1 + \left(2 \cdot 10^4 \left(\frac{\varepsilon}{D}\right) + \frac{10^6}{Re}\right)^{\frac{1}{3}}\right]$	Moody (1947)[38]
$f = -2\log_{10}\left[\left(\frac{\frac{\varepsilon}{D}}{3.7065}\right) - \left(5.0452 \cdot \frac{A}{Re}\right)\right]$ where: $A = \log_{10}\left[\frac{\left(\frac{\varepsilon}{D}\right)^{1.1098}}{2.8257} + \frac{5.8506}{Re^{0.8981}}\right]$	Chen (1979)[41]
$f = -2\log_{10}\left[\left(\frac{\varepsilon/D}{3.7}\right) - \frac{5.0.2 \cdot B}{Re}\right]$ where: $A = \log_{10}\left[\frac{\varepsilon/D}{3.7} + \frac{13}{Re}\right]$, $B = \log_{10}\left[\frac{\varepsilon/D}{3.7} - \frac{5.02 \cdot A}{Re}\right]$	Zigrang & Sylvester (1982)[42]
$f = -2\log_{10}\left[\left(\frac{\frac{\varepsilon}{D}}{3.7065}\right) - \left(5.0272 \cdot \frac{B}{Re}\right)\right]$ where: $B = \log_{10}\left[\frac{\frac{\varepsilon}{D}}{3.827} - \left(\frac{4.567A}{Re}\right)\right]$, $A = \log_{10}\left[\left(\frac{\frac{\varepsilon}{D}}{7.7918}\right)^{0.9924} + \left(\frac{5.3326}{208.815 + Re}\right)\right]$	Monzon-Romeo-Royo (2002)[43]

literature expressions over the entire range of Reynolds number. The fitting formula has been adjusted to the friction factor equations with a least squares method based on the Zigrang & Sylvester correlation[42].

To demonstrate the accuracy of this expression, Equation. (11) is plotted in Figure 3 together with the expressions of Table 2 for a large range of Reynolds number (covering both laminar regimes with Re<2300 and turbulent ones) and for two extreme $\frac{\varepsilon}{D}$ ratios (0.0001 and 0.01) that bound the typical range in compressors for refrigeration and heat pump systems.

The proposed correlation closely follows the calculations of the four expressions. Moreover, it provides almost identical results with the Monzon-Romeo-Royo correlation[43] for both relative roughness values. It should be highlighted that this expression is the most recent from the available literature and includes all previous findings on this topic.

Finally, in order to integrate Equation. (11) in the suction pressure drop calculations, it is preferred not to use the Reynolds number as the independent variable, whose calculation includes the effective diameter of the suction port, which is an unknown. Instead, a similar parameter to the Reynolds number is used, which considers only the mass flow rate and the viscosity. This is achieved by multiplying the Reynolds number with the constant term $\left(\frac{\pi D}{4}\right)$, as shown in Equation. (12). The final correlation of the friction factor is given by Equation. (13).

$$X = \frac{\pi D Re}{4} = \frac{\dot{m}_{r,cp,su3}}{\mu} \quad (12)$$

$$f(X) = A'_0 + A'_1 (\log_{10}(X))^{-3} \quad (13)$$

Where μ is the fluid viscosity, D is the suction port diameter and A'_0 and A'_1 are the adjusted parameters that include the geometrical values that impact on suction pressure drop and are introduced to the set of the model parameters to be determined by the Θ function minimization (Table 1).

As a result, the initial constant friction factor is replaced with the expression of Equation. (13), introducing an additional parameter to the model, and leading to 13 parameters in total. The verification of this approach will be presented in a next section.

Testing facilities of a vapour injection compressor

The tested vapour injection compressor is the Copeland ZH13KVE-TFD scroll compressor provided for R407C (GWP= 1980, ODP=0) with 11.7 m^3/h displacement at 50 Hz. This compressor is for heating applications and is equipped with an economizer port to allow the operation with vapour injection. The developed heat pump includes this compressor and the design work resulted in using R1234ze(E) with GWP =4 (20-years GWP)[44] and ODP=0 as drop-in replacement, expecting a heating COP reduction less than 10% compared with the same compressor running with R407C. The heat pump testing aimed to primarily examine and evaluate the reliability and performance of the compressor, with the heat pump to be later integrated in a prototype domestic heating application.

Comparison of refrigerants R407C and R1234ze(E)

In order to overview the main characteristics of R1234ze(E) compared to R407C, the thermodynamic properties at 0 °C and 50 °C are shown in Table 3. The calculations have been performed within EES (Engineering Equation Solver) software[31], which includes integrated thermodynamic libraries of the examined refrigerants. R407C has higher latent heat and lower specific volume at both lower and higher temperatures, indicating a higher capacity and a more compact system.

Concerning the operational envelope of the compressor, which is originally provided for R407C, this is transposed for R1234ze(E), by converting the compressor's pressure ranges to the corresponding temperatures. The original for R407C and the adjusted for R1234ze(E) envelopes are shown in Figure 4. The heat pump with R1234ze(E) was tested near the lower limits of the envelope with lower suction pressure levels and reduced efficiency.

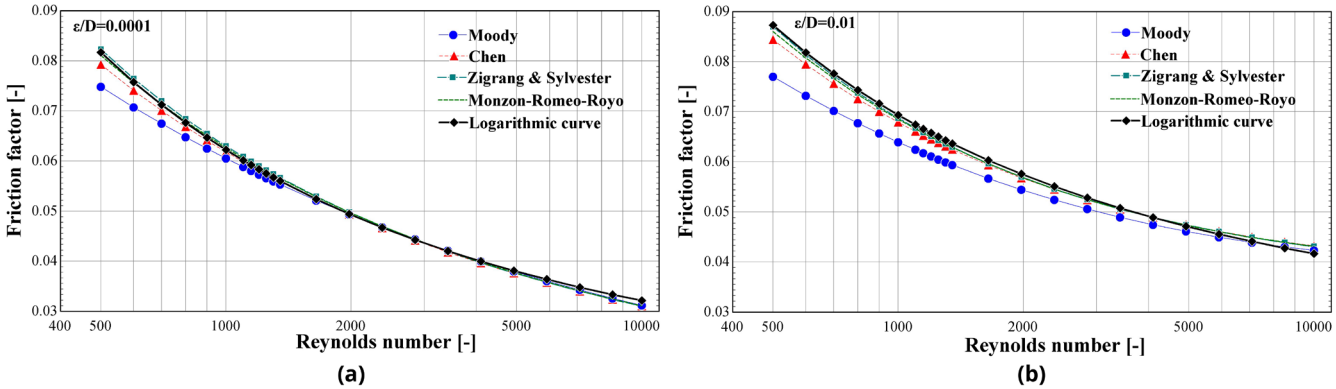


Figure 3. Friction factor as calculated by the proposed equation and the expressions of Table 2 over a large range of Reynolds numbers and for two ε/D ratios: (**a**) 0.0001; and (**b**) 0.01.

Table 3. Thermo-physical properties of the two refrigerants.

Refrigerant	Thermo-physical properties									
	Latent heat (kJ kg^{-1})		Specific Volume (m^3/kg)		Sat. liquid specific heat (kJ kg^{-1}K^{-1})		Sat. vapor specific heat (kJ kg^{-1}K^{-1})		Critical Temperature (°C)	Critical Pressure (Bar)
	0 °C	50 °C	0 °C	50 °C	0 °C	50 °C	0 °C	50 °C		
R407C	209.3	149.1	0.051	0.011	1.42	1.78	0.96	1.47	86.2	46.32
R1234ze(E)	184.2	145.1	0.084	0.018	1.34	1.51	0.90	1.15	109.4	36.32

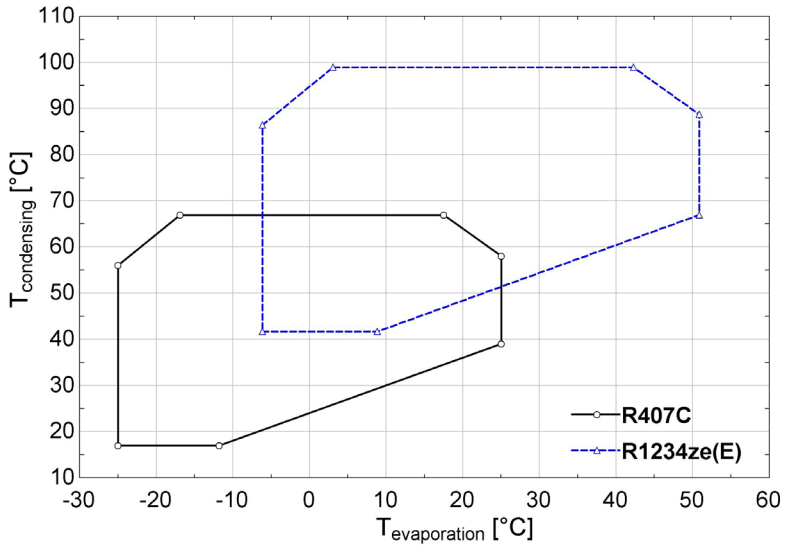


Figure 4. Compressor performance envelope of the Copeland ZH13KVE-TFD scroll compressor with R407C and R1234ze(E) refrigerant.

Description of the heat pump test-rig

The experimental setup consists of a vapour compression heat pump for heating designed for R1234ze(E) and charged with a total refrigerant amount of 4 kg (supplied by Honeywell/ Solstice® ZE). All three heat exchangers (HEX) are of plate type. Their sizing and selection was based on the manufacturer's software of SWEP taking into consideration both input-output temperatures and water mass flow rates provided by previous simulation results. Also, an over-surfacing of 25% has been applied in order to ensure that the performance of the HEX is kept always within the design conditions. As a result, model B25TH with 20 plates and 1.13 m^2 of heat exchange area has been selected for both condenser and evaporator, but with different couplings and dimensions for the inlet/outlet connections. For the economizer, model B5TH was selected, with 34 plates and a surface of 0.384 m^2.

The injection mass flow is determined by a thermostatic expansion valve placed at the condenser outlet, which provides some control of the superheat, keeping it within the range of 3–10 K. The selected expansion valve was the Danfoss T2/TE2 134 model and the control spring pressure was adjusted for the operation with R1234ze(E) by shifting the superheat compared to R134a according to the manufacturer. Concerning the superheat control at the compressor suction an electronic expansion valve (EEV) was preferred, and the one selected is produced by PARKER, type CEV24-S. The controller of this valve processes the measured temperature and pressure at the evaporator's outlet and accordingly a series of electrical pulses are sent to the stator of the EEV causing to open or to close. The preferred control mechanism is a PID loop keeping the superheat in a very close range to the setpoint, equal to about 3 K. Moreover, a receiver with a volume of 1.5 l has been used produced by OCS (type RV1CC102X210) to account for changes in the operating conditions. After the receiver, a filter (GMC 5/8" SC165MM) is placed with a nominal volume of 250 cm^3. The developed heat pump installed at the laboratory during the tests is shown in Figure 5, indicating the main components.

The heat pump also includes two pumps for the water circulation between the heat exchangers and the water tanks.

The water flow at the condenser is adjusted by controlling the pump speed with a low-voltage PWM (pulse-width modulation) signal. The maximum flow rate of the circulator pump is 4 m^3/h and head of 7 m with a power consumption below 60 W (Grundfos, type ALPHA1 L 15-65 130). For the evaporator water circuit, a booster pump has also been installed in series, ensuring that the flow rate is adequate. In this circuit, a circulator pump with permanent magnet motor (Grundfos, type MAGNA 3) is used with a maximum flow rate of 12 m^3/h and head of 10 m, delivering higher mass flow rates that can achieve lower water temperature differences.

The secondary circuits for the hot and cold side of the heat pump are connected to a different insulated water tank with a volume of 5 m^3 each. Concerning the tank temperature control, the evaporator water tank is equipped with electric resistors for heating up the stored water. On the other hand, the water tank connected to the condenser is equipped with an air-source heat pump to cool the water in the tank. By doing so, the inlet water temperatures to the heat pump can be stabilized at both evaporator and condenser, allowing for test to be performed with constant supply conditions. For a better overview, the piping and instrumentation diagram of the vapour injection heat pump is depicted in Figure 6, showing both the components and the measurement points.

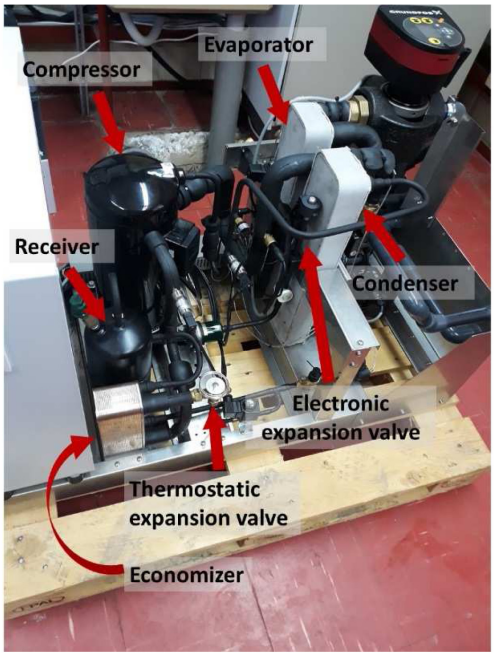


Figure 5. The heat pump tested at the laboratory.

Sensors and their accuracy

Various sensors are installed for measuring the pressure of the refrigerant and the temperature of both the refrigerant and water at different parts of the cycle. In total, there are three pressure sensors and 10 temperature sensors (six for the refrigerant and four for the water lines). All measurements related to the refrigerant are collected and recorded by the Programmable logic controller (PLC) unit of the heat pump with a sampling rate of one minute.

Moreover, a power meter (Siemens, type SICAM T 7KG9661) measures the total electrical consumption of the heat pump. The measurements that are collected at the water side as well as the (indoor) ambient temperature and the total power consumption is recorded by a data logger (Agilent, type 34972A) with a sampling rate once every 30 seconds. These are then synchronized with the ones recorded by the PLC unit of the heat pump.

The sensors of the experimental setup together with their range and accuracy are presented in Table 4, given separately for the heat pump (by the PLC) and the test-rig sides (by the data logger).

Test conditions

All tests have been conducted with the evaporator inlet temperature ranging from 10 up to 25 °C while the water outlet of the condenser ranged from 32 to 55 °C. The tests

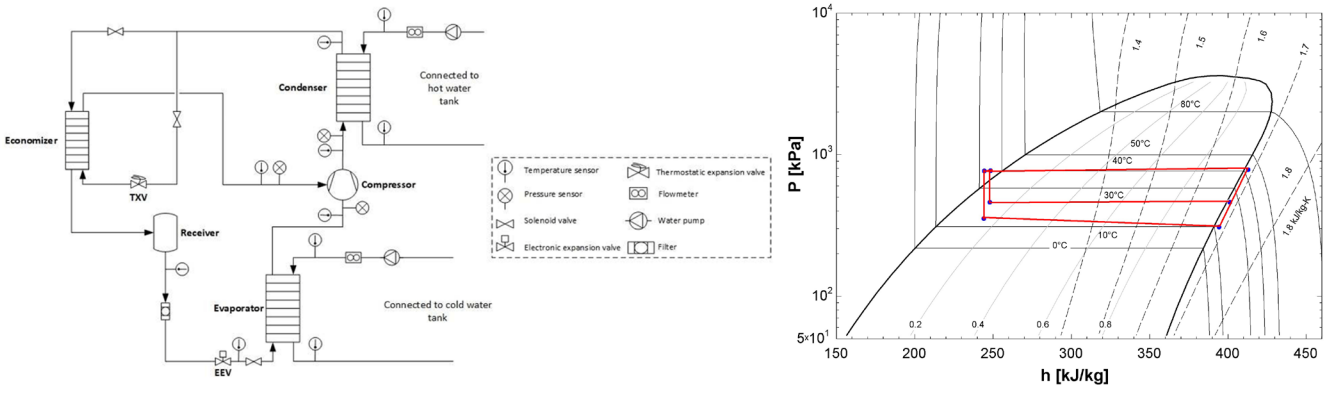


Figure 6. (**a**) Schematic diagram of the tested heat pump with measurement points, (**b**) The corresponding P-h diagram.

Table 4. Accuracy and range of heat pump sensors and meters.

Meter/Sensor	Quantity	Type	Range	Accuracy
Test-rig				
Water flow meter (condenser)	1	Yokogawa ADMAG AFX electromagnetic flow meter	Adjustable (0–20,000 lt/h)	<1%
Water flow meter (evaporator)	1	Krohne IFC 010D electromagnetic flow meter	Adjustable (1–15,000 lt/h)	<1%
Water temperature	4	PT100, 4-wire	0–100 °C	0.1 K
Power meter	1	Siemens Sicam-T	0–50 kW per phase (with current transformers)	0.5%
Heat pump				
Refrigerant temperature	6	PT100, 3-wire	-20 – +80 °C	0.1 K
Refrigerant gauge pressure	3	Pressure transmitter ESCP-MIT1	0–10 bar for the evaporator and economizer lines 0–30 bar for the condenser line	0.25% of FS
Water temperature	4	PT100, 3-wire	0 – 100 °C	0.1 K

were performed at constant water flow rates (1.35 m^3/h at the condenser and 2.18 m^3/h at the evaporator) and with a constant compressor frequency of 50 Hz. Three main testing sets have been obtained regarding the temperature range of the evaporator and condenser, by keeping the evaporator water inlet temperature at three temperature scales 10, 15 and 25 °C respectively, while the condenser water outlet is varied from 32 to about 55 °C with a constant elevating trend, since the heat pump was delivering heat to a large tank.

At the beginning of every testing set, the heat pump was operating to bring the temperature of the evaporator water tank to the desired level with simultaneous operation of the outdoor air-source heat pump, in order to reduce the water temperature of the condenser tank. As the water temperature of the evaporator's tank was stabilized by adjusting the operation of the electric resistances, the water temperature of the condenser tank started to increase until it reached the maximum set-point of 55 °C.

The heat pump was operating many hours per day (six to eight) only for experimental reasons and for consecutive days (about 3 weeks), recording all measured data and controlling the temperatures of the tanks. As a sample, Figure 7 shows the refrigerant temperatures and pressures during six hours of testing, when the water at the evaporator tank was maintained at about 25 °C while the condenser tank was heated from 45 up to 55 °C.

All collected measurements have been synchronised with a sampling rate of 1 minute, and then they were time-averaged into 10-minute steps. The final dataset is determined by selecting several such 10-minute sets with the measured values having small fluctuations during this averaging process. A small fluctuation is defined here as 1-minute measurements with a deviation of less than 5% compared to the 10-minute averaged value in terms of temperatures and pressures. Table 5 summarizes the range of the final measurement points that are taken into consideration, in order to evaluate the compressor and the overall heat pump performance.

Data reduction

The key performance indicators and energy flows are calculated from the measured temperatures, pressures, flow rates and power consumption. The heating capacity (Q_c) is identified from the water-side of the condenser as in Reference 45 given by Equation. (14), assuming no heat losses in order to enable the calculation of the refrigerant mass flow rate ($\dot{m}_{r,c}$). Due to the lack of mass flow meters at the refrigerant side of the test rig, it is not possible to carry out confirmation tests for the heat rate balance on the water and refrigerant side respectively. However, the heat exchangers are sufficiently insulated and as a result it is assumed that no heat is lost in the HEX.

$$Q_c = \dot{m}_{w,c} \cdot c_{p,w,c} \cdot \Delta T_{w,c} = \dot{m}_{r,c} \cdot (h_{r,c,in} - h_{r,c,out}) \quad (14)$$

where $\dot{m}_{w,c}$ is the measured water mass flow rate, $c_{p,w}$ is the specific heat capacity, and ΔT_w is the water temperature difference between the outlet and inlet port of the plate heat exchanger.

The total mass flow rate at the condenser, which is the discharge mass flow of the compressor, is calculated by an energy balance at the water side (first part of Equation. (14)). The refrigerant enthalpies at the condenser's outlet ($h_{r,c,out}$) and inlet ($h_{r,c,in}$) are calculated by the measured pressures and temperatures. The heating COP is calculated by Equation. (15).

$$COP = \frac{Q_c}{\dot{W}_{cp}} \quad (15)$$

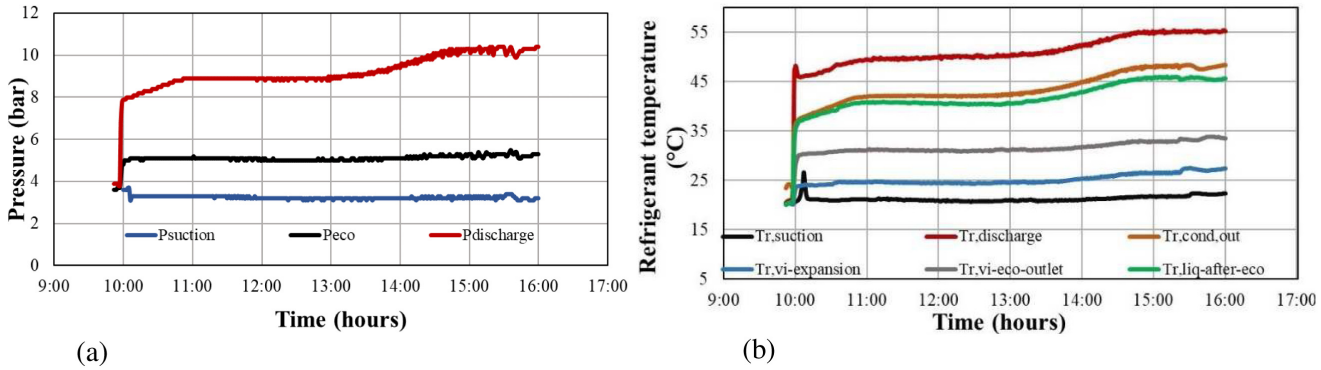


Figure 7. Sample of the refrigerant-side measured data for a six-hour heat pump operation: (**a**) refrigerant pressures; (**b**) refrigerant temperatures.

Table 5. Main test conditions of the heat pump.

Property	Value
Refrigerant suction pressure (relative) (bar)	1.7 – 3.5
Refrigerant discharge pressure (relative) (bar)	6.24 – 11.6
Water inlet temperature to evaporator (°C)	9.82 – 26.66
Water outlet temperature from condenser (°C)	31.55 – 55.01
Total power consumption (kW)	2.23 – 3.09

where $\dot{W}_{cp}$ is the compressor electric power, which is equal to the electric power measured by the power meter including all power consumptions once reduced by the power consumption of all secondary components such as pumps, controllers etc.

Except from COP, the 2nd law efficiency is also be used as an indicator of how much of the theoretical Carnot (maximum) efficiency is achieved. According to Reference 46 the 2nd law efficiency (η_{II}, also called Carnot efficiency) is defined as the ratio of the required minimum energy input for an ideal system, to the actual energy input of the real system, given by Equation. (16).

$$\eta_{II} = \frac{COP}{COP_{ideal}} \tag{16}$$

where COP_{ideal} is the COP of the Carnot cycle which is related only with the temperature levels of the heat pump supply and sink (water) side.

The performance indicators of the compressor are the volumetric and isentropic efficiency identified by Equation. (6) and Equation (7) as it was proposed in a characterization methodology of a vapour injection scroll compressor[34]. In Equation. (6), the refrigerant mass flow rate is identified at this time by applying an energy balance at the evaporator, similar to Equation. (13). Moreover, by using the continuity equation (Equation. (3)) and once the evaporator and condenser mass flow rates are determined, the vapour injection mass flow is then calculated. This enables the identification of the isentropic efficiency with the use of Equation. (7).

This processing method leads to the calculation of the key performance indicators. The selected operating conditions include 13 datasets. These have been obtained from the collected ones directly from the measurement points and then the heat losses and pressure drop in the piping have been considered, in order to form the final inlet and outlet conditions of each component. Further the data were screened and selected based on the minimum fluctuations of the measured values over the 10-minute period. The measured data of the heat pump are provided in Table 6, and will be used for the semi-empirical model calibration in the next section.

Also, the main processed properties such as the suction and vapour injection mass flows, are identified from the previous analysis using the provided data of Table 6. The performance indicators of the heat pump are calculated from the same dataset by means of Equation. (6)–Equation. (7) with the results presented in Table 7.

Uncertainty analysis and final data set

In order to adequately analyse the obtained data set, an uncertainty analysis is provided using EES software[31]. According to Reference 47,48, in order to calculate the propagation of sensors accuracy through the calculated properties, the systematic error (ε) of a given calculated value (y) is identified by Equation. (17).

$$\varepsilon_y = \sqrt{\sum_i \left(\frac{\partial y}{\partial x_i}\right)^2 \varepsilon_{x_i}^2} \tag{17}$$

where $\varepsilon_{\chi i}$ is the measurement uncertainty of the independent variables and $\frac{\partial y}{\partial x_i}$ the partial derivative of the function y with respect to every independent variable χ_i.

Table 6. **Final measured dataset of the heat pump.**

Ambient temperature (°C)	Suction temperature (°C)	Discharge temperature (°C)	Condenser outlet temperature (°C)	Receiver Liquid temperature (°C)	Vapour injection temperature (°C)	Suction pressure (bar)	Vapour injection pressure (bar)	Discharge pressure (bar)	Compressor power (W)
23.5±0.1	19.0±0.1	38.8±0.1	28.1±0.1	28.3±0.1	26.7±0.1	4.00±0.02	5.60±0.02	7.24±0.07	2292.00±11.46
20.8±0.1	19.2±0.1	44.5±0.1	35.7±0.1	34.8±0.1	28.3±0.1	4.00±0.02	5.63±0.02	8.63±0.07	2468.00±12.34
21.3±0.1	21.0±0.1	50.6±0.1	42.8±0.1	41.0±0.1	31.2±0.1	4.17±0.02	6.03±0.02	10.02±0.07	2679.00±13.40
21.7±0.1	21.8±0.1	55.1±0.1	48.2±0.1	45.8±0.1	32.8±0.1	4.23±0.02	6.25±0.02	12.25±0.07	2851.00±14.26
27.9±0.1	23.1±0.1	58.7±0.1	51.4±0.1	49.4±0.1	35.6±0.1	4.20±0.02	6.65±0.02	11.96±0.07	3034.00±15.17
27.1±0.1	23.7±0.1	59.8±0.1	52.5±0.1	50.5±0.1	36.6±0.1	4.26±0.02	6.79±0.02	12.26±0.07	3076.00±15.38
26.9±0.1	13.5±0.1	41.6±0.1	33.0±0.1	30.5±0.1	23.8±0.1	2.12±0.02	4.61±0.02	7.64±0.07	2248.00±11.24
26.5±0.1	16.0±0.1	47.7±0.1	40.3±0.1	37.3±0.1	27.5±0.1	2.41±0.02	5.08±0.02	9.02±0.07	2529.00±12.65
34.0±0.1	13.7±0.1	54.2±0.1	49.4±0.1	45.6±0.1	36.4±0.1	2.11±0.02	5.15±0.02	10.82±0.07	2701.00±13.51
31.7±0.1	14.8±0.1	58.1±0.1	53.6±0.1	49.8±0.1	42.8±0.1	2.21±0.02	5.42±0.02	12.08±0.07	2850.00±14.25
28.6±0.1	9.9±0.1	49.3±0.1	44.2±0.1	39.9±0.1	34.4±0.1	2.74±0.02	4.65±0.02	9.53±0.07	2470.00±12.35
29.4±0.1	9.8±0.1	49.3±0.1	44.2±0.1	40.0±0.1	34.5±0.1	2.70±0.02	4.64±0.02	9.54±0.07	2469.00±12.35
31.3±0.1	11.5±0.1	54.1±0.1	49.6±0.1	45.7±0.1	39.0±0.1	2.90±0.02	4.89±0.02	10.88±0.07	2669.00±13.35

Open Research Europe 2022, 2:49 Last updated: 13 NOV 2024

Table 7. Processed data of the heat pump.

Compressor suction mass flow rate (kg/s)	Vapour injection mass flow rate (kg/s)	Isentropic efficiency (-)	Volumetric efficiency (-)
0.0651±0.0023	0.0060±0.0014	0.36±0.01	0.91±0.03
0.0609±0.0025	0.0082±0.8150	0.42±0.16	0.86±0.03
0.0613±0.0026	0.0093±0.0016	0.45±0.01	0.83±0.03
0.0593±0.0027	0.011±0.0017	0.46±0.01	0.79±0.03
0.0547±0.0027	0.0138±0.0017	0.43±0.01	0.74±0.04
0.0552±0.0028	0.0141±0.0018	0.44±0.01	0.74±0.04
0.0417±0.0024	0.0093±0.0015	0.38±0.01	0.75±0.04
0.0424±0.0025	0.0119±0.0016	0.39±0.01	0.70±0.04
0.0237±0.0028	0.0147±0.0017	0.31±0.02	0.43±0.05
0.0206±0.0029	0.0166±0.0018	0.29±0.02	0.36±0.05
0.0198±0.0026	0.0135±0.0016	0.29±0.02	0.41±0.05
0.0199±0.0026	0.0135±0.0016	0.29±0.02	0.41±0.05
0.0178±0.0028	0.0158±0.0017	0.28±0.02	0.34±0.05

Using Equation. (17) and taking into account the accuracies of Table 5, the uncertainties of the processed data are then calculated and are shown in Table 6 and Table 7.

Results and discussion

The processed test results of the heat pump are initially presented over a sufficient range of temperatures. After that, the results of the verified semi-empirical model are given, identifying the compressor losses and their magnitude.

Experimental results with R1234ze(E)

In this section, the experimental results of the heat pump configuration with R1234ze(E) are presented for variable condenser and evaporator temperatures. The test data (Table 6) are used to determine the capacities of the components, for evaluating the overall system performance and compared with the operation with R407C based on the manufacturer data.

The delivered condenser heat for variable temperatures is depicted in Figure 8. The maximum heating capacity is 11 kW (50% lower compared to R407C) for evaporator inlet water temperature of 25 °C, while the minimum is observed for high temperature lifts between supply and sink temperatures ($\Delta T>30$ K) providing a heating capacity of 4 kW at the maximum lift of 45 K. On the other hand, the capacity seems not to be affected with R407C for the same evaporation temperature level, with the increase becoming more significant as the temperature lift increases.

The heating capacity is also highly affected by the supply temperature level, which drastically varies the mass flow rate. The suction mass flow rate is reduced by over 8% when the temperature lift increases from 20 to 30 K for an evaporator temperature of 25 °C while the same reduction for an evaporator temperature of 15 °C is over 25%. On the other hand, the vapour injection mass flow rate is increased by at least 23% for these temperature lifts. Despite the contribution of the vapour injection, the total mass flow rate is lower than the expected. According to manufacturer performance data provided for R407C there is an observed mass flow decrease of over 50% for similar operating conditions with the experimental ones.

The electricity consumption of the compressor of the heat pump is depicted in Figure 9, and indicates that it increases in an almost linear way when the pressure ratio is elevated (higher temperature lifts). This is a reasonable trend, since for higher pressure ratios the power requirements are increased in order to achieve the desirable discharge pressure. This leads to an increase of the vapour injection mass flow rate, accordingly reducing the suction flow rate. Also, from Figure 9 is clear that the compressor underperforms with R1234ze(E) since for the same operating conditions, the power consumption with R407C is 0.6-1 kW greater. This follows the significantly lower capacity observed in Figure 8, due to the lower refrigerant mass flow rates.

The heat pump performance is expressed through the COP, considering the compressor power only. The power of all auxiliaries (water pumps, inverter losses, etc.) has also been measured and is equal to about 140 W. The compressor COP together with the 2nd law efficiency are presented in Figure 10 for the same operating conditions as before (Figure 9).

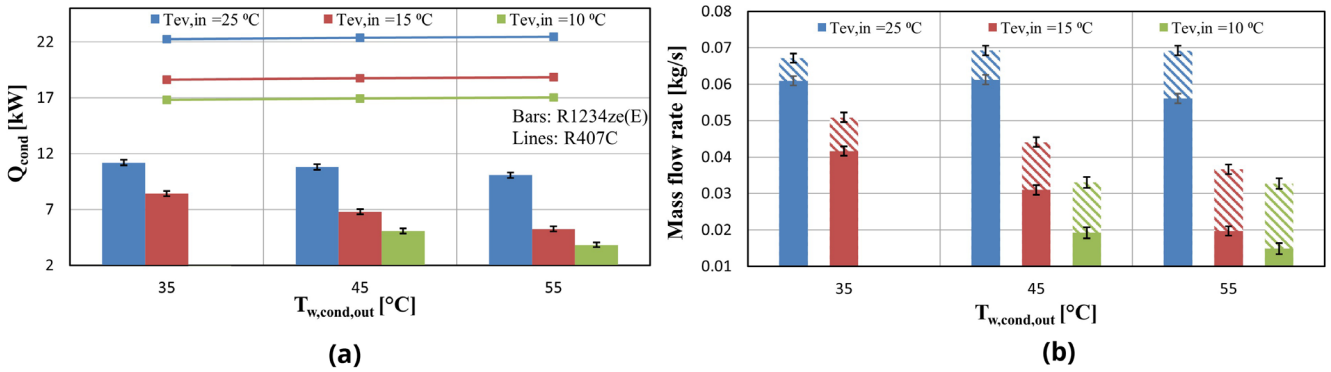


Figure 8. Condenser heat and compressor mass flow rates for the two refrigerants at three water supply temperature levels for variable condenser water temperature: (**a**) Condenser heat; (**b**) Compressor mass flow rate at the evaporator (solid bars) and vapor injection mass flow rate (dashed bars).

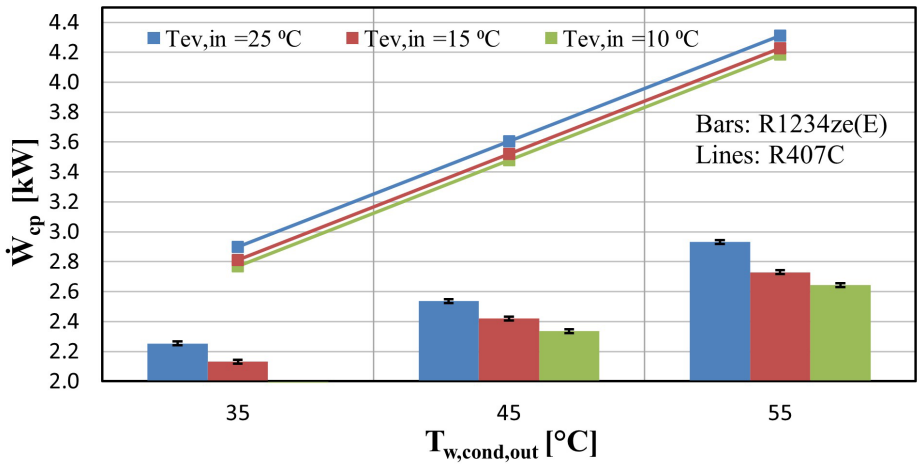


Figure 9. Compressor power ($\dot{W}_{cp}$) for the two refrigerants at three water supply temperature levels and for variable water condenser temperature.

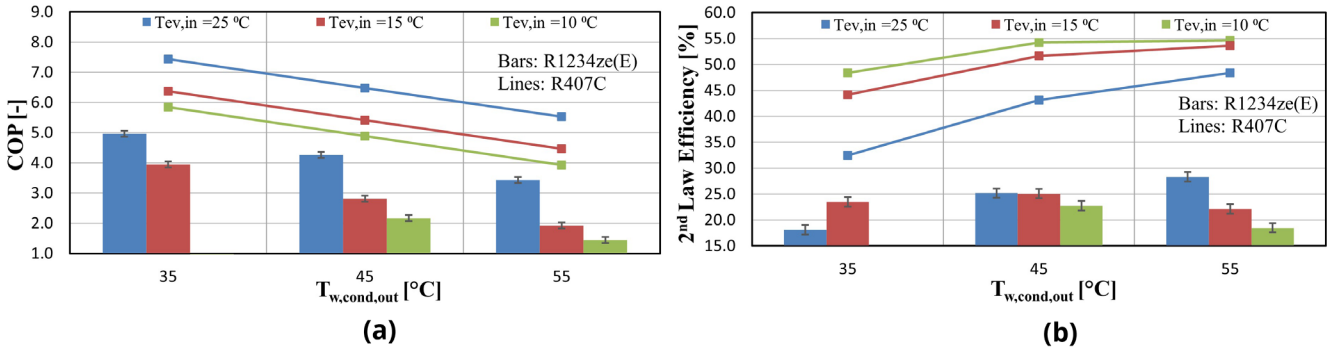


Figure 10. Compressor coefficient of performance (COP) and 2nd law efficiency for the two refrigerants at three water supply temperature levels for variable water condenser temperature: (**a**) COP; (**b**) 2nd law efficiency.

The heat pump reaches a maximum COP of 5 for a low lift of 10 K, whereas for a lift of 20 K the COP is about 4 for all condenser temperatures. For the same temperature lifts, the COP values based on the manufacturer data are 7.1 and 5.5 respectively. For high-temperature lifts of over 40 K the COP is decreased reaching values below 2, which is much lower

than expected (about 4 with R407C). The 2nd law efficiency assists in evaluating the low performance of the compressor. This efficiency is in the range of 18.1–28.33%, while it is increased to about 40–50% with the same compressor when using R407C, which is a typical value[49].

According to the initial design work of the system concerning the compressor selection procedure, the COP was expected to be decreased by 5–10% compared with R407C, but the test results revealed a much lower performance, with the COP being 50% lower than expected. The reasons behind this are going to be identified and explained later, using the developed semi-empirical model.

Results of the developed semi-empirical model with vapour injection

The developed model is initially calibrated and its results compared with the available data from the manufacturer with R407C and the same compressor (ZH13KVE) for verification purposes. As a second step, the model is fine-tuned based on the test data, identifying the main reasons for underperformance.

Vapour injection semi-empirical model verification with R407C. The operating conditions consider a suction superheat of 10 K, condenser subcooling of 3 K, and frequency of 50 Hz. By doing so, 36 operating datasets[50] are extracted, covering compressor suction temperatures from -15 to 25 °C and condensing temperatures from 25 to 60 °C, all within the compressor envelope.

The semi-empirical model parameters are then fine-tuned[37], when using the standard suction pressure drop model (with a constant friction factor) and the improved model (with the logarithmic correlation presented previously).

The calibration work resulted in the same values of the parameters with the standard and improved suction pressure drop models, with the exception of the two friction factor parameters. The values of all parameters are shown in Table 8.

Significant heating of the refrigerant at the suction is observed, since the suction heat transfer coefficient is one order of magnitude higher than the other two heat transfer coefficients. In addition, there is an over-estimation of the swept volume of the compressor by 5.6%, which is also observed in the findings of relevant literature[27,30,33]. This is because the identified swept volume does not correspond to the actual one, but considers several other processes. The built-in volume ratio $r_{v,in}$, is also an identified parameter of the model and represents the ideal volume ratio of the compressor.

Due to the compatibility of R407C and the examined compressor with all operating conditions included in the envelope, the suction fluid flow is a fully developed turbulent flow. This is identified by the parameter values of the logarithmic expression for suction pressure drop that gives an almost constant friction factor, and thus expecting the results of the two models to be similar. Specifically, the A_1' parameter is related to the logarithmic part of Equation. (13) and is two orders of magnitude lower than the A_0', which represents the constant part of the correlation with a value similar to the constant friction factor (K).

The results of the semi-empirical model using the standard and improved models for suction pressure drop are depicted in Figure 11–Figure 13 comparing the calculated mass flow rate, the electric power and the discharge temperature of R407C with all available data from the manufacturer. The 5% margins for electric power and mass flow rate and 3 K margin for the discharge temperature are also indicated.

Table 8. Semi-empirical model parameters with vapour injection and R407C.

Parameter	Sub-processes	Standard suction pressure drop	Improved suction pressure drop	Units
$AU_{amb,cp}$	Heat transfer coefficient for heating-up during supply	12.6		W/K
$AU_{ex,cp,n}$	Heat transfer coefficient for heat loss during the exhaust	11.72		W/K
$AU_{su,cp,n}$	Heat transfer coefficient for heat losses to the ambient	218.7		W/K
$A_{leak,\ cp}$	Effective area of leakages	6.41E-08		m^2
$\dot{W}_{loss0,cp}$	Constant term of the electrical power losses	276.1		W
a_{cp}	Coefficient of the variable term of the electrical power losses	0.227		-
$V_{s,cp}$	Swept volume of the compressor	71.03		cm^3
$r_{v,in}$	Built-in volume ratio of the compression	3.54		-
K	Lumped friction factor parameter	3.99E+08	-	$1/m^4$
A_0'	Constant term of the friction factor correlation adjusted parameter	-	3.401E+08	$1/m^4$
A_1'	Variable term of the friction factor correlation adjusted parameter	-	5.114E+06	$1/m^4$

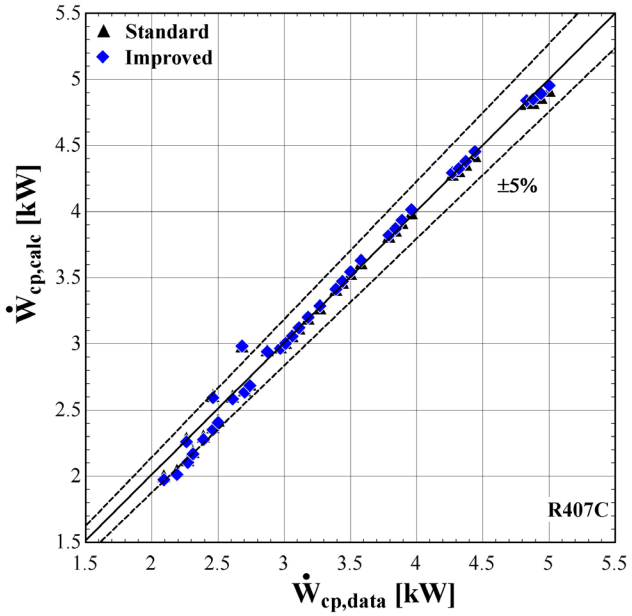


Figure 11. Comparison of the calculated electrical power, $\dot{W}_{cp,calc}$ (with the standard and improved suction pressure drop) with the available one ($\dot{W}_{cp,data}$).

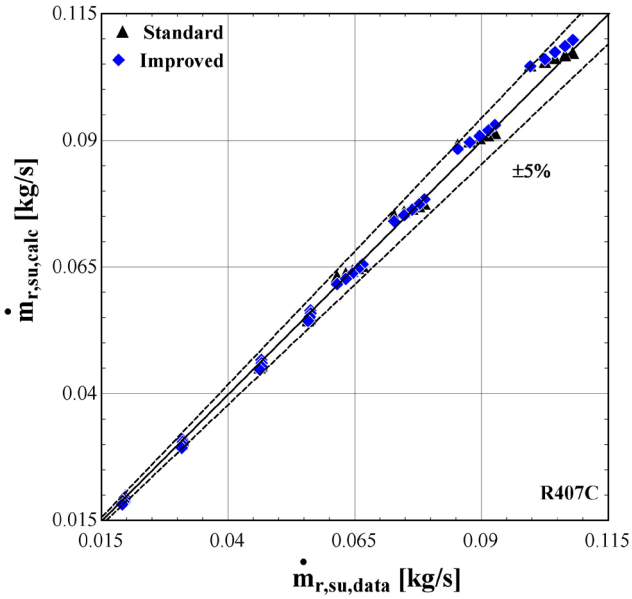


Figure 12. Comparison of the calculated mass flow rate, $\dot{m}_{r,su,calc}$ (with the standard and improved suction pressure drop) with the available one ($\dot{m}_{r,su,data}$).

As shown in Figure 11, the electric power prediction for the compressor is sufficiently calculated for the whole range, keeping the deviation within ±5% for the majority of testing points, observing very few diversions. These are to be expected, since the calibration process has been accomplished for a very large range of conditions. However, the electric power prediction for moderate and high values is almost identical to the available one. This is achieved for both standard and improved suction pressure drop models, since the mass flow rate and refrigerant velocity is increased, assuring the fully developed flow of the refrigerant.

As far as the mass flow rate is concerned, the prediction is always within a 5% margin showing better accuracy for low

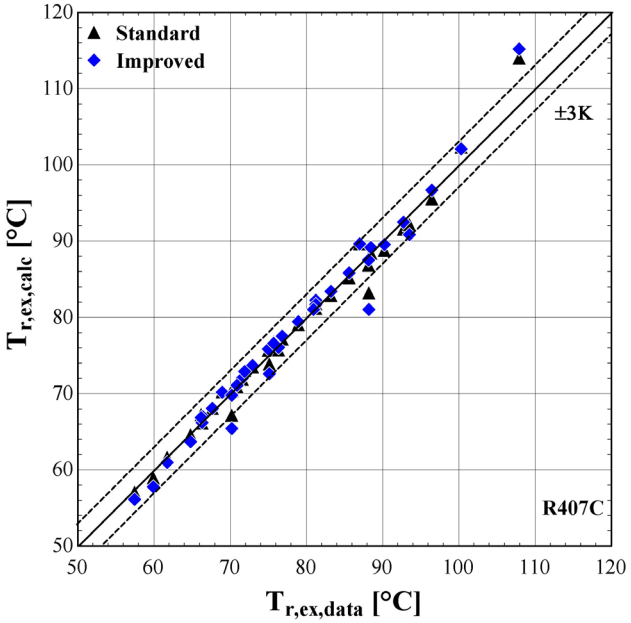


Figure 13. Comparison of the calculated discharge temperature, $T_{r,ex,calc}$ (with the standard and improved suction pressure drop) with the available one ($T_{r,ex,data}$).

and moderate rates (below 0.07 kg/s). Comparing the results of the standard and improved suction pressure drop models, it is evident that there is no clear improvement since the values are almost identical.

Finally, the discharge temperature is adequately calculated with most of the operating conditions within the 3 K range. Only two conditions of moderate discharge temperature and one of high temperature exceed the ±3 K limit, being underestimated by almost 6 K. This discrepancy can be explained because these points are characterized by very low evaporating temperatures (below -10 °C) and are located in the boundaries of the compressor envelope making it very challenging for the model to accurately predict the behaviour. The results of the two suction pressure drop models are similar, with the improved model having a better accuracy for moderate temperatures in the range of 70–90 °C.

The minimum, maximum and average deviation of the predicted variables for both standard and improved suction pressure drop model are presented in Table 9.

Although there are a few values that have greater deviations than the defined limits, in all cases the average error is kept below 2% for the mass flow rate and electric power respectively, and 1.07 K for the discharge temperature. The accuracy of the two suction pressure drop models seems to be the same with negligible differences, as indicated by the average deviations of Table 9.

Finally, the verification of the developed model is proved by the low deviation values for the main properties. These deviations could be even lower, if the range of the conditions were restricted, for example by considering compressor suction temperatures from -10 to 15 °C and condensing temperatures from 40 to 60 °C. Moreover, the results of the two suction pressure drop models are almost identical, indicating that the use of the improved model does not bring any improvements at these specific conditions.

Semi-empirical model calibration to experimental data with R1234ze(E) and the effect of suction pressure drop. The vapour injection semi-empirical model is then calibrated with the use of the test data. The inputs concern the refrigerant suction pressure and temperature, the discharge pressure and the vapour injection pressure, temperature and mass flow rate (Table 6 and Table 7). This calibration process is followed for both the standard and improved suction pressure drop approach. The fine-tuned values of all parameters are given in Table 10, which significantly differ from the ones for R407C presented in Table 8.

The suction's overall heat transfer coefficient is rather low, leading to a minor heating up of the refrigerant by about 1–2 K. This is because the mass flow rate of the vapour injection is increased, reducing at the same time the suction flow rate. Also, overall heat transfer coefficient of the discharge is high, which enhances the heat losses of the compressed refrigerant, although the ambient temperature was even 30 °C in some cases.

In addition, the electric compressor losses are also higher with R1234ze(E) than with R407C, presenting a 76% increment on the constant electrical losses factor ($\dot{W}_{loss0,cp}$) and an increase

Table 9. Minimum, maximum, and average deviation of the predicted variables of the semi-empirical model compared with the available data for R407C.

	Discharge temperature deviation (K)			Mass flow rate deviation (%)			Electric power deviation (%)		
	Min	Max	Average	Min	Max	Average	Min	Max	Average
Standard model	-5.88	5.06	1.07	-4.47	3.43	1.77	-11.30	6.96	1.99
Improved model	-5.41	5.43	1.06	-5.52	2.61	1.54	-11.23	6.85	1.97

Table 10. Semi-empirical model parameters with vapour injection and R1234ze(E).

Parameter	Sub-processes	Standard suction pressure drop	Improved suction pressure drop	Units
$AU_{amb,cp}$	Heat transfer coefficient for heating-up during supply	1600		W/K
$AU_{ex,cp,n}$	Heat transfer coefficient for heat loss during the exhaust	320.8		W/K
$AU_{su,cp,n}$	Heat transfer coefficient for heat losses to the ambient	10.02		W/K
$A_{leak,\ cp}$	Effective area of leakages	1.77E-07		m^2
$\dot{W}_{loss0,cp}$	Constant term of the electrical power losses	487.8		W
α_{cp}	Coefficient of the variable term of the electrical power losses	0.5496		-
$V_{s,cp}$	Swept volume of the compressor	63.43		cm^3
$r_{v,in}$	Built-in volume ratio of the compression	4.726		-
K	Lumped friction factor parameter	8.35E+08	-	$1/m^4$
A'_0	Constant term of the friction factor correlation adjusted parameter	-	-2.3975E+10	$1/m^4$
A'_1	Variable term of the friction factor correlation adjusted parameter	-	1.2593E+12	$1/m^4$

of over 100% for the variable losses factor (α_{cp}). This was expected to some extent, since the constant inverter losses of the tested compressor with R1234ze(E) are included in the measured electric power. Moreover, the energy balance at the compressor's shell imposes a very high heat transfer coefficient at the casing. This could indicate that the assumption of the isothermal wall with a constant temperature is not entirely valid, and possibly the shell should be split into two regions (top and bottom), each with a different envelope temperature.

The friction factor of the standard suction pressure drop approach has a similar value to the case with R407C (although two times higher). On the other hand, the improved model gives a parameter of the logarithmic part two orders of magnitude greater than the constant part, revealing a significant variation in the friction factor as the evaporation temperature changes. This will become clearer later in this work, when the compressor losses are examined.

Figure 14 – Figure 16 compare the model results of the standard and improved friction factor approach with the measured data.

The electric power calculated by the improved model (Figure 13) seems to be consistent with the experimental results always staying within the ±5%. Moreover, the majority of examined conditions are closer to the experimental data than the data obtained using the standard model.

The standard suction pressure drop introduces large deviations to the mass flow rate, especially for the lower values, whereas for moderate/high flow rates (in the range of 0.04–0.06 kg/s) the results are similar to the measured ones. On the other hand, the improved suction pressure drop model reduces the discrepancies in the whole range. Especially for the lower mass flow rates, the error is significantly reduced, with the calculations ranging within the ±5% bandwidth. For the moderate mass flow rates, the logarithmic trend of the suction

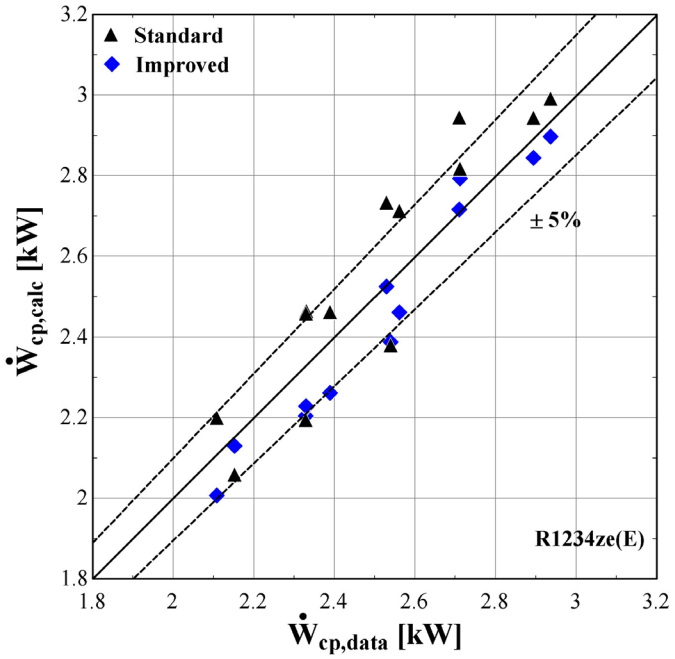


Figure 14. Comparison of the calculated electrical power, $\dot{W}_{cp,calc}$ (with the standard and improved suction pressure drop) with the measured one ($\dot{W}_{cp,data}$).

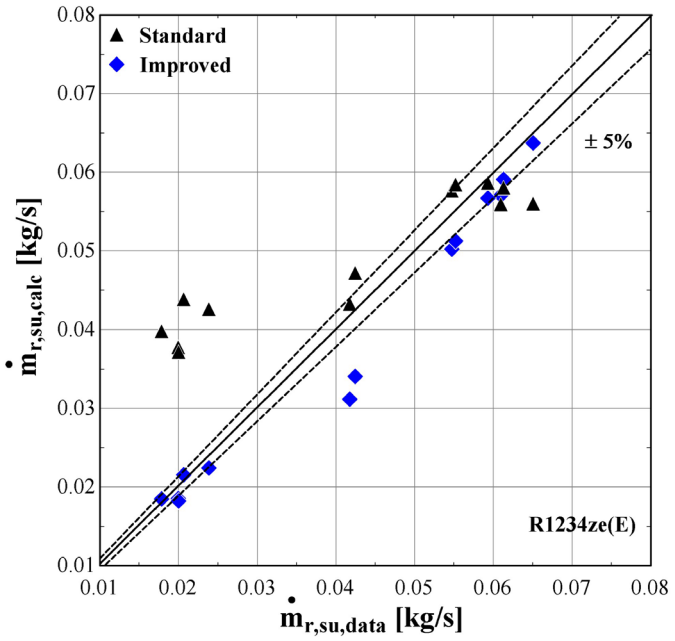


Figure 15. Comparison of the calculated mass flow rate, $\dot{m}_{r,su,calc}$ (with the standard and improved suction pressure drop) with the measured one ($\dot{m}_{r,su,data}$).

pressure drop seems to be less accurate, showing a maximum underestimation of about 25%. This can be explained from the calibration process that aims to minimize the total error, with the algorithm compromising between reaching a lower accuracy for these conditions and a higher accuracy for conditions within low and high mass flow regions.

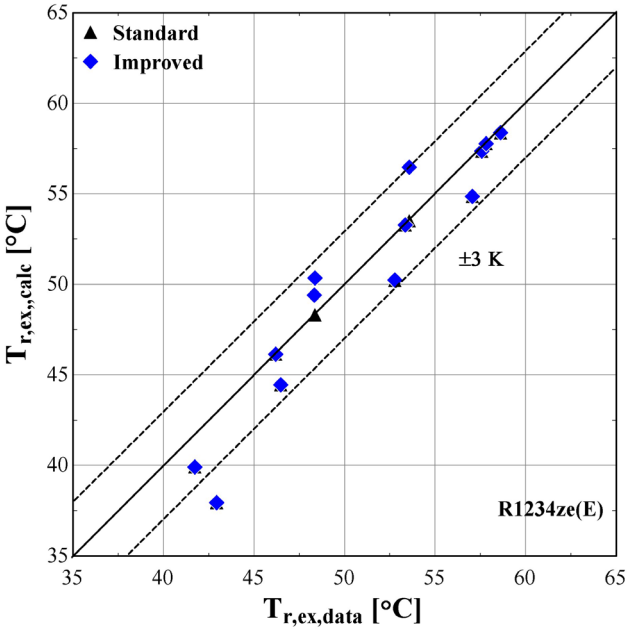


Figure 16. Comparison of the calculated discharge temperature, $T_{r,ex,calc}$ (with the standard and improved suction pressure drop) with the measured one ($T_{r,ex,data}$).

The calculated discharge temperature with the two suction pressure drop models show similar results, with a small deviation from the measured values. The majority of examined conditions are within the ±3 K range, except for one that almost reaches a 5 K underestimation and corresponds to an extreme condition with a very low pressure ratio and temperature lift (discharge temperature of 43 °C).

In order to further examine the impact of the improved model on the overall prediction accuracy, the isentropic and volumetric efficiencies are calculated and presented in Figure 17, the trendline of each dataset is also shown (3rd order polynomial for the isentropic efficiency and 2nd order polynomial for the volumetric efficiency, also well approached with a linear correlation).

Both standard and improved friction factor models adequately predict the isentropic efficiency in a pressure ratio range from 1.5 to 3. This range corresponds to higher mass flow rates with a low suction pressure drop. For higher pressure ratios, the accuracy of the improved model improves, with its results closely following the experimental data that reach an isentropic efficiency of just 30%.

Regarding the volumetric efficiency, the standard model only provides adequate accuracy for low pressure ratios (below 2.5), while its calculations lead to a constant volumetric efficiency for all conditions, equal to about 85%, instead of declining with the pressure ratio, with the maximum deviation exceeding 140%. The results of the improved model are very close to the experimental values for the whole operating range, capturing the linear reduction of the volumetric efficiency with the pressure ratio. Finally, the very low volumetric efficiency of even 40% is the result of the high suction pressure drop, being the main cause of the compressor underperformance, as will be discussed later.

The previous outcomes are supported by the minimum, maximum and average deviations of the three key properties considering the two suction pressure drop correlations, given in Table 11.

The deviation of the discharge temperature is about the same for both cases, and similarly for the electric power. However, the mass flow rate deviation is significantly decreased when using the improved suction pressure drop approach, as the average deviation is reduced by 75%, compared to the standard model. This indicates that the new model approach for suction pressure drop recreates the experimental points more accurately, since for pressure ratios above 2.5 the flow is closer to a laminar one with high friction factor rather than the standard turbulent conditions. Therefore, the improved model will be used from now on, so that to evaluate the compressor losses with a higher accuracy.

Compressor losses. The previous analysis leads to identifying the losses mechanisms, which are related to the pressure drop, heat losses and electrical losses. Figure 18 presents the suction pressure drop of the same compressor with R407C and R1234ze(E), when using the improved model. In order to perform an impartial comparison between the two refrigerants, a subset of the initial data set of R407C is obtained, which

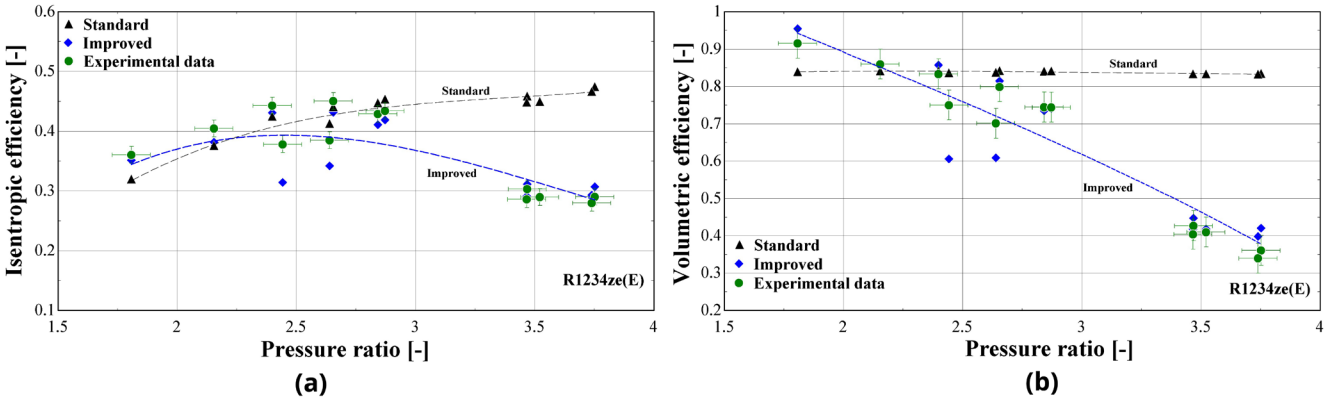


Figure 17. Comparison of the calculated efficiencies (with the standard and improved suction pressure drop) with the available ones from the test data: (**a**) Isentropic efficiency; (**b**) Volumetric efficiency.

Table 11. Minimum, maximum and average deviation of the predicted variables of the semi-empirical model with standard and improved suction pressure drop approach compared to the measured data with R1234ze(E).

	Discharge temperature deviation (K)			Mass flow rate deviation (%)			Electric power deviation (%)		
	Min	Max	Average	Min	Max	Average	Min	Max	Average
Standard	0.05	4.98	1.10	-123.0	14.00	41.80	-8.63	6.29	5.01
Improved	-2.90	4.98	1.54	-4.46	25.34	8.20	-3.02	5.95	3.20

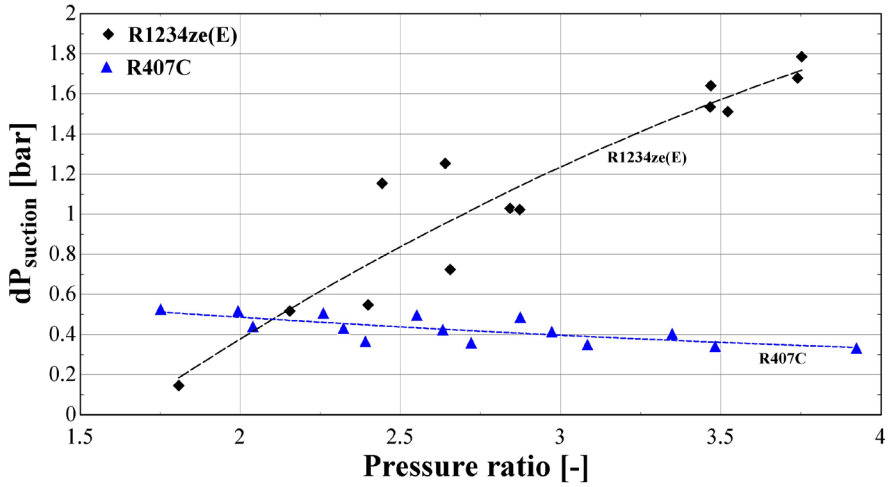


Figure 18. Calculated suction pressure drop ($dP_{suction}$) of R407C and R1234ze(E) as a function of the pressure ratio.

corresponds to the same range of evaporating and condensing temperatures with the test data of R1234ze(E).

The suction pressure drop with R1234ze(E) ranges from about 0.2 bar for low temperature lifts, reaching 1.8 bar for a pressure ratio of 3.8. This drop is very high and has a significant impact on the refrigerant density, leading to a very low volumetric efficiency, as presented in Figure 17. On the other hand, the pressure drop of R407C varies within a reasonably small range (0.3-0.6 bar), and slightly decreases for larger

pressure ratios. It should be highlighted that the discharge pressure drop of the two refrigerants is similar and always lower than 0.2 bar. This drop is within the reported values found in the literature[29,49], and has a negligible impact on the compressor performance.

The above results reveal the main reason for compressor underperformance which is related to the low suction pressure of R1234ze(E) for low evaporation temperatures. The suction pressure is about 3–4 bar less than with R407C for the same temperature levels (although the pressure ratio range is very similar), indicating that the flow approaches the laminar regime due to a reduced fluid velocity and Reynolds number, increasing, in that case, the friction factor as presented previously. The result is a very high pressure drop at the suction line of the compressor, resembling the operation of a choking valve that imposes the refrigerant to flow through the alternative path of the vapor injection line. This is depicted in Figure 19 and shows the measured and calculated suction mass flow rate and the mass flow rate ratio (vapour injection-VI to suction flow) as a function of the suction pressure for R1234ze(E) refrigerant.

The ratio between injected and suction mass flow rate of R1234ze(E) is extremely high reaching about 80% at low suction pressure and temperature, whereas it reduces to typical values of about 20–30% for a lower pressure ratio. This is still rather high compared with the one of R407C that ranges from about 7 to 36%.

Apart from the pressure losses, the energy flows of the compressor are examined. These are related to the energy balance at the fictitious isothermal wall (negative values once leaving the shell, positive ones to the shell), involving the suction heat gain, discharge heat loss, ambient heat losses and electrical losses. These are presented in Figure 20 for both R1234ze(E) and R407C.

The thermal and electrical losses with R1234ze(E) are significantly higher compared with the ones of R407C, which

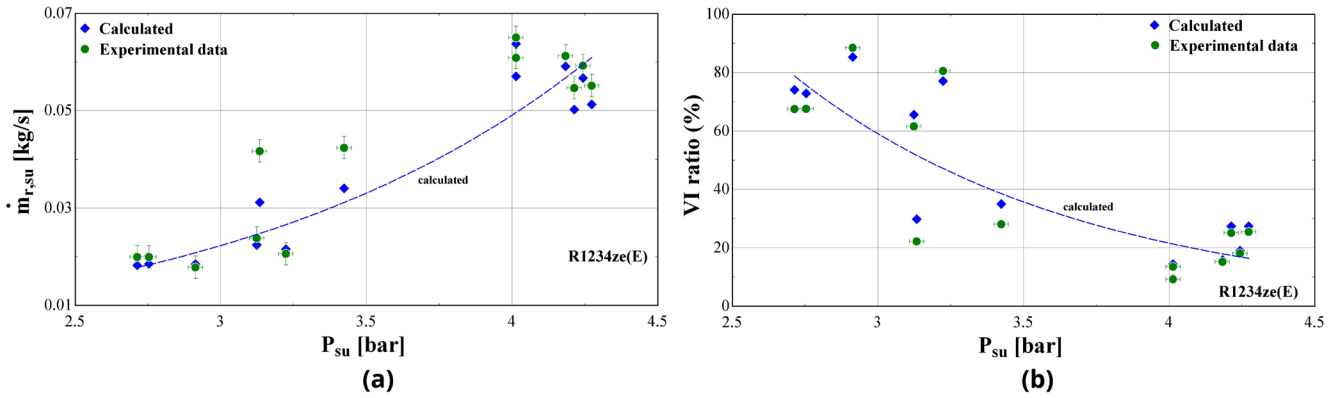


Figure 19. Suction mass flow rate ($\dot{m}_{r,su}$) and vapour injection mass flow rate ratio (VI ratio) as a function of the suction pressure (P_{su}) of R1234ze(E): (**a**) Suction mass flow rate; (**b**) Vapour injection mass flow rate ratio.

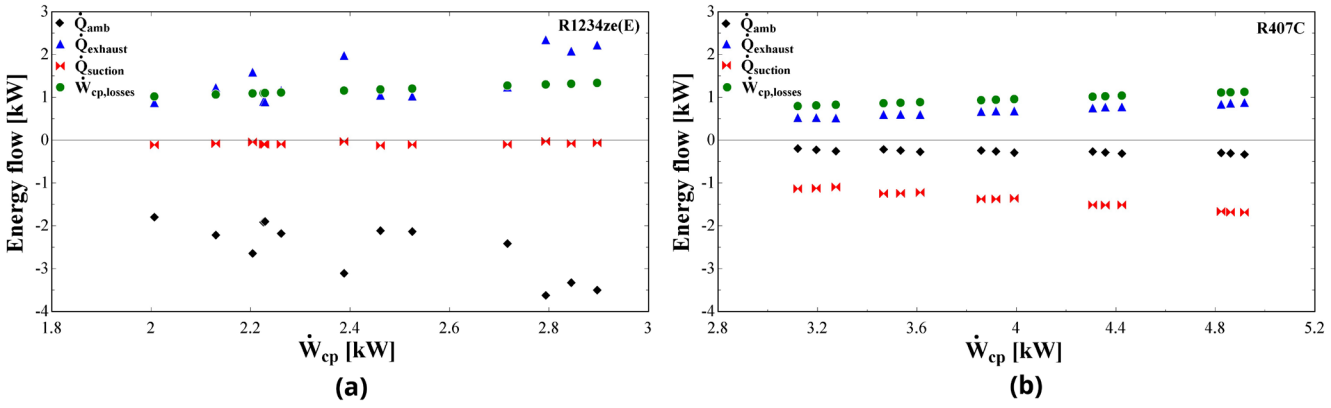


Figure 20. Energy flows (heat losses to the ambient: $\dot{Q}_{amb}$, heat losses to the exhaust: $\dot{Q}_{exhaust}$, heat gain at the suction: $\dot{Q}_{suction}$, compressor losses: $\dot{W}_{cp,losses}$) at the fictitious isothermal wall as a function of the compressor power ($\dot{W}_{cp}$): (**a**) R1234ze(E); (**b**) R407C.

is a direct outcome of the higher parameter values identified during the model calibration (Table 7 and Table 9). Almost all variables are linearly related to the compressor work with R407C, while both thermal and electrical losses are in close agreement with the results presented in Reference 32.

The heat transfer at the suction in the case of R1234ze(E) has a minor effect on the overall energy balance with negligible heating of the refrigerant. This is not the case with R407C, for which the 35% of the compressor power heats the supplied refrigerant. Moreover, the electrical losses have a linear dependency on the compressor work and their values are about the same for both refrigerants and range between 0.8 and 1.3 kW. However, the relative electrical losses are much lower with R407C, due to its higher compressor power.

The heat transfer at the exhaust as well as the ambient losses with R1234ze(E) dominate the energy balance applied to the compressor casing. The cooling down of the refrigerant takes values from 0.9 to 2.3 kW which corresponds to 45–76% of the total compressor work, while this fraction is reduced for R407C to 10–20%. This reveals that due to the significant pressure drop of R1234ze(E) the temperature is reduced and only a small fraction of the total supplied energy is transferred to the refrigerant. In addition, the heat of the R1234ze(E) cooling down and the electrical losses are practically transferred to the surrounding environment, since their sum is about the same with the ambient losses which are in the range of 1.9-3.6 kW. These losses are much lower for R407C, due to the minor refrigerant cooling down and the increased suction heating up, as it was mentioned before.

Conclusions

An experimental setup of a vapour injection scroll compressor of a heat pump has been presented. This water-to-water heat pump is for heating only and designed for R1234ze(E) refrigerant. The testing procedure focused on a wide variety of operating conditions with the water supply temperatures ranging from 10 °C to 25 °C and sink temperatures from 32 °C to 55 °C. The test results were evaluated, revealing that the compressor was not performing as expected, especially for high temperature lifts ($\Delta T>30$ K). At such conditions, the heating capacity was drastically reduced accompanied by a significant decrease in the COP, which reached values below 2. This underperformance was also identified by the values of the 2nd law efficiency that reached a maximum of just 28.33%.

In order to identify the main causes of this and examine with detail the losses mechanisms, a semi-empirical model for scroll compressors with vapour injection has been developed by the authors, including an improved version of the suction pressure drop approach that considers both the laminar and turbulent flow regimes. The accuracy of this model has been verified based on the same compressor with R407C, with the standard and improved model for the suction pressure drop giving similar results. This is because the suction mass flow rate is high enough so that the inlet fluid flow remains turbulent over the whole range of suction temperatures. The next step included the semi-empirical model calibration based on the experimental tests with R1234ze(E). Comparing the predicted values of the model with the experimental ones, it was shown that the discharge temperatures are sufficiently estimated with a deviation lower than ±5 K for both the standard and improved model, with a similar accuracy for the electric power. However, the greatest improvement, in the improved model, is observed to the suction mass flow rate, since the error is reduced by almost 80% compared with the constant friction factor approach. The analysis shows that the properties of R1234ze(E) related to a lower suction pressure and density reduce the flow velocity and Reynolds number, with the flow approaching (or reaching) the laminar regime, increasing the friction factor and triggering the large pressure losses at the suction line, which become up to five times higher than the ones of R407C.

Furthermore, the energy balance at the fictitious isothermal wall of the compressor was examined for both refrigerants further enlightening the reasons for compressor underperformance with R1234ze(E). The thermal and electrical losses with R1234ze(E) are significantly higher compared with the losses of R407C including increased cooling down of the refrigerant at the discharge as well as very high ambient losses. Moreover, although the simulation with R407C led to 60% higher compressor power for similar operating conditions, the electrical losses were about the same with R1234ze(E), something that further decreased the overall compressor performance. As a result, only a small fraction of the total supplied energy is transferred to the refrigerant and the parameter values of the semi-empirical model divert from the typical ones of the literature, in order for the compressor to be modelled with the highest possible accuracy.

Overall, the proposed semi-empirical model for scroll compressor with vapour injection is verified with the improved correlation for suction pressure drop modelling, increasing both the physical background and prediction accuracy. This enables the prediction of the key properties of the compressor when operating at unexplored conditions even outside the envelope and with refrigerants that no performance data exist, with the final outcome to locate the losses related to the pressure drop, heat transfer and electrical consumption.

Ethics and consent

Ethical approval and consent were not required.

Nomenclature

A	Area of heat exchanger	m^2
A'_0	Constant parameter of the improved model	m^{-4}
A'_1	Parameter of the logarithmic part of the improved model	m^{-4}
c_p	Specific heat capacity	$kJ \cdot kg^{-1}K^{-1}$
D	Diameter	m
f	Darcy-Weisbach friction factor	-
h	Enthalpy	$kJ \cdot kg^{-1}$

K	Friction factor parameter	m^{-4}
$\dot{m}$	Mass flow rate	$kg \cdot s^{-1}$
N	Compressor speed	s^{-1}
P	Pressure	bar
Q	Heat	kW
R	Ratio	-
Re	Reynolds number	-
T	Temperature	°C
U	Overall heat transfer coefficient	$kW \cdot m^{-2}K^{-1}$
u	Velocity	$m \cdot s^{-1}$
V	Volume	m^3
$\dot{V}$	Volumetric flow rate	$m^3 \cdot s^{-1}$
v	Specific volume	$m3 \cdot kg^{-1}$
w	Specific work	$kJ \cdot kg^{-1}$
$\dot{W}$	Electrical power	kW
X	Modified Reynolds number	m
Z	Number of data sets	-

Greek symbols

α	Compressor losses variable term	-
Δ	Difference	-
ε	Relative roughness	m
η	Efficiency	-
Θ	Optimization parameter	-
μ	Dynamic viscosity	Pa·s
ρ	density	$kg \cdot m^{-3}$

Subscripts

0	Initial value
ad	Adapted conditions
amb	Ambient
c	Condenser
calc	Calculated value
cp	Compressor
data	Obtained value
ev	Evaporator
ex	Exhaust
in	Internal or inlet
inj	Injection
int	Intermediate
is	Isentropic
leak	Leakage
loss	Compressor losses
n	Nominal
out	Outlet
r	Refrigerant
s	Swept
su	Suction
v	Volumetric, isochoric
vi	Vapour injection
vol	Volumetric
w	Wall

Abbreviations

COP	Coefficient of performance
EES	Engineering equation solver
GWP	Global warming potential
HC	Hydrocarbon
HEX	Heat exchanger
HFC	Hydrofluorocarbon
HFCO	Hydrochlorofluoroolefin
HFO	Hydrofluoroolefin
HTHP	High temperature heat pump
IHX	Internal heat exchanger
ODP	Ozone depletion potential
PLC	Programmable logic controller
PWM	Pulse Width Modulation
VI	Vapour injection

Data availability

Underlying data

Zenodo: Test and numerical data of a vapour-injection scroll compressor in a heat pump with R1234ze(E), [Dataset] https://doi.org/10.5281/zenodo.5785939[50].

This project contains the following underlying data:

- Test and simulation data_Compressor_with_VI_R1234ze(E).xlsx (all data used to produce the results of this study).

Data are available under the terms of the Creative Commons Zero "No rights reserved" data waiver (CC0 1.0 Public domain dedication).

References

1. Schulz M, Kourkoulas D: **Regulation (EU) No 517/2014 of The European Parliament and of the Council of 16 April 2014 on Fluorinated Greenhouse Gases and Repealing Regulation (EC) No 842/2006.** 2014.
Reference Source

2. Höglund-Isaksson L, Purohit P, Amann M, *et al.*: **Cost Estimates of the Kigali Amendment to Phase-down Hydrofluorocarbons.** *Environ Sci Policy.* 2017; **75**: 138–147.
Publisher Full Text

3. Mota-Babiloni A, Navarro-Esbrí J, Barragán-Cervera Á, *et al.*: **Analysis Based on EU W No 517/2014 of New HFC/HFO Mixtures as Alternatives of High GWP Refrigerants in Refrigeration and HVAC Systems.** *Int J Refrig.* 2015; **52**: 21–31.
Publisher Full Text

4. Wu D, Hu B, Wang RZ: **Vapor Compression Heat Pumps with Pure Low-GWP Refrigerants.** *Renew Sustain Energy Rev.* 2021; **138**: 110571.
Publisher Full Text

5. Mota-Babiloni A, Navarro-Esbrí J, Molés F, *et al.*: **A Review of Refrigerant R1234ze(E) Recent Investigations.** *Appl Therm Eng.* 2016; **95**: 211–222.
Publisher Full Text

6. Zilio C, Brown JS, Schiochet G, *et al.*: **The Refrigerant R1234yf in Air Conditioning Systems.** *Energy.* 2011; **36**(10): 6110–6120.
Publisher Full Text

7. Życzkowski P, Borowski M, Łuczak R, *et al.*: **Functional Equations for Calculating the Properties of Low-GWP R1234ze(E) Refrigerant.** *Energies.* 2020; **13**(12): 3052.
Publisher Full Text

8. Gil B, Szczepanowska A, Rosiek S: **New HFC/HFO Blends as Refrigerants for the Vapor-Compression Refrigeration System (VCRS).** *Energies.* 2021; **14**(4): 946.
Publisher Full Text

9. Mota-Babiloni A, Navarro-Esbrí J, Barragán Á, *et al.*: **Drop-in Energy Performance Evaluation of R1234yf and R1234ze(E) in a Vapor Compression System as R134a Replacements.** *Appl Therm Eng.* 2014; **71**(1): 259–265.
Publisher Full Text

10. Janković Z, Sieres Atienza J, Martínez Suárez JA: **Thermodynamic and Heat Transfer Analyses for R1234yf and R1234ze(E) as Drop-in Replacements for R134a in a Small Power Refrigerating System.** *Appl Therm Eng.* 2015; **80**: 42–54.
Publisher Full Text

11. Colombo LPM, Lucchini A, Molinaroli L: **Experimental Analysis of the Use of R1234yf and R1234ze(E) as Drop-in Alternatives of R134a in a Water-to-Water Heat Pump.** *Int J Refrig.* 2020; **115**; 18–27.
Publisher Full Text

12. Mendoza-Miranda JM, Mota-Babiloni A, Ramírez-Minguela JJ, *et al.*: **Comparative Evaluation of R1234yf, R1234ze(E) and R450A as Alternatives to R134a in a Variable Speed Reciprocating Compressor.** *Energy.* 2016; **114**: 753–766.
Publisher Full Text

13. Wu H, Lin K, Huang H, *et al.*: **Research on Effects of Vapor Injection on Twin-Screw Compressor Performance.** *Int J Refrig.* 2020; **118**: 483–490.
Publisher Full Text

14. Xu X, Hwang Y, Radermacher R: **Refrigerant Injection for Heat Pumping/Air Conditioning Systems: Literature Review and Challenges Discussions.** *Int J Refrig.* 2011; **34**: 402–415.
Publisher Full Text

15. Liu H, Nagano K, Katsura T, *et al.*: **Experimental Investigation on a Vapor Injection Heat Pump System with a Single-Stage Compressor.** *Energies.* 2020; **13**(12): 3133.
Publisher Full Text

16. Yang M, Wang B, Li X, *et al.*: **Evaluation of Two-Phase Suction, Liquid Injection and Two-Phase Injection for Decreasing the Discharge Temperature of the R32 Scroll Compressor.** *Int J Refrig.* 2015; **59**: 269–280.
Publisher Full Text

17. Lumpkin DR, Bahman AM, Groll EA: **Two-Phase Injected and Vapor-Injected Compression: Experimental Results and Mapping Correlation for a R-407C Scroll Compressor.** *Int J Refrig.* 2018; **86**: 449–462.
Publisher Full Text

18. Winandy EL, Lebrun J: **Scroll Compressors Using Gas and Liquid Injection: Experimental Analysis and Modelling.** *Int J Refrig.* 2002; **25**(8): 1143–1156.
Publisher Full Text

19. Cho H, Chung JT, Kim Y: **Influence of Liquid Refrigerant Injection on the Performance of an Inverter-Driven Scroll Compressor.** *Int J Refrig.* 2003; **26**(1): 87–94.
Publisher Full Text

20. Wang X, Hwang Y, Radermacher R: **Two-Stage Heat Pump System with Vapor-Injected Scroll Compressor Using R410A as a Refrigerant.** *Int J Refrig.* 2009; **32**(6): 1442–1451.
Publisher Full Text

21. Xu S, Fan X, Ma G: **Experimental Investigation on Heating Performance of Gas-Injected Scroll Compressor Using R32, R1234yf and Their 20wt%/80wt% Mixture under Low Ambient Temperature.** *Int J Refrig.* 2017; **75**: 286–292.
Publisher Full Text

22. Shuxue X, Guoyuan M: **Experimental Study on the Characteristics of Scroll Compressor with Vapor Injection for Electric Vehicles Air Conditioning.** In *Proceedings of the 12th IEA Heat Pump Conference* 2017; O.3.2.2.
Reference Source

23. Fukuda S, Kondou C, Takata N, *et al.*: **Low GWP Refrigerants R1234ze(E) and R1234ze(Z) for High Temperature Heat Pumps.** *Int J Refrig.* 2014; **40**: 161–173.
Publisher Full Text

24. Kosmadakis G, Arpagaus C, Neofytou P, *et al.*: **Techno-Economic Analysis of High-Temperature Heat Pumps with Low-Global Warming Potential Refrigerants for Upgrading Waste Heat up to 150° C.** *Energy Convers Manag.* 2020; **226**: 113488.
Publisher Full Text

25. Wang B, Shi W, Li X, *et al.*: **Numerical Research on the Scroll Compressor with Refrigeration Injection.** *Appl Therm Eng.* 2008; **28**(5–6): 440–449.
Publisher Full Text

26. Park YC, Kim Y, Cho H: **Thermodynamic Analysis on the Performance of a Variable Speed Scroll Compressor with Refrigerant Injection.** *Int J Refrig.* 2002; **25**(8): 1072–1082.
Publisher Full Text

27. Dardenne L, Fraccari E, Maggioni A, *et al.*: **Semi-Empirical Modelling of a Variable Speed Scroll Compressor with Vapour Injection.** *Int J Refrig.* 2015; **54**: 76–87.
Publisher Full Text

28. Cho IY, Ko SB, Kim Y: **Optimization of Injection Holes in Symmetric and Asymmetric Scroll Compressors with Vapor Injection.** *Int J Refrig.* 2012; **35**(4): 850–860.
Publisher Full Text

29. Tello-Oquendo FM, Navarro-Peris E, Barceló-Ruescas F, *et al.*: **Semi-Empirical Model of Scroll Compressors and Its Extension to Describe Vapor-Injection Compressors. Model Description and Experimental Validation.** *Int J Refrig.* 2019; **106**: 308–326.
Publisher Full Text

30. Winandy E, Saavedra C, Lebrun J: **Experimental Analysis and Simplified Modelling of a Hermetic Scroll Refrigeration Compressor.** *Appl Therm Eng.* 2002; **22**(2): 107–120.
Publisher Full Text

31. Klein SA: **Engineering Equation Solver-EES (64-Bit)**. Version 10.834. Academic Professional 2020.

32. Cuevas C, Lebrun J: **Testing and Modelling of a Variable Speed Scroll Compressor.** *Appl Therm Eng.* 2009; **29**(2–3): 469–478.
Publisher Full Text

33. Cuevas C, Lebrun J, Lemort V, *et al.*: **Characterization of a Scroll Compressor under Extended Operating Conditions.** *Appl Therm Eng.* 2010; **30**(6–7): 605–615.
Publisher Full Text

34. Tello-Oquendo FM, Navarro-Peris E, Gonzálvez-Maciá J: **New Characterization Methodology for Vapor-Injection Scroll Compressors.** *Int J Refrig.* 2017; **74**: 528–539.
Publisher Full Text

35. Bahman AM, Ziviani D, Groll EA: **Vapor Injected Compression with Economizing in Packaged Air Conditioning Systems for High Temperature Climate.** *Int J Refrig.* 2018; **94**: 136–150.
Publisher Full Text

36. ASHRAE ANSI/ASHRAE Standard 23.1: **Method of Testing for Rating the Performance of Positive Displacement Refrigerant Compressor and Condensing Units That Operate at Subcritical Temperatures of the Refrigerant.** 2015.

37. Meramveliotakis G, Kosmadakis G, Karellas S: **Methods Based on a Semi-Empirical Model for Simulating Scroll Compressors with HFC and HFO Refrigerants [version 2; peer review: 1 approved].** *Open Res Eur.* 2021; **1**: 148.
Publisher Full Text

38. Moody LF: **An Approximate Formula for Pipe Friction Factors.** *Trans ASME.* 1947; **69**: 1005–1006.

39. Asker M, Turgut OE, Coban MT: **A Review of Non Iterative Friction Factor Correlations for the Calculation of Pressure Drop in Pipes.** *Bitlis Eren Univ J Sci & Technol.* 2014; **4**: 1–8.
Reference Source

40. Colebrook CF: **Turbulent Flow in Pipes, with Particular Reference to the Transition Region between the Smooth and Rough Pipe Laws.** *J Inst Civil Engineers.* 1939; **11**(4): 133–156.
Publisher Full Text

41. Chen NH: **An Explicit Equation for Friction Factor in Pipe.** *Ind Eng Chem Fundamen.* 1979; **18**(3): 296–297.
Publisher Full Text

42. Zigrang DJ, Sylvester ND: **Explicit Approximations to the Solution of Colebrook's Friction Factor Equation.** *Aiche J.* 1982; **28**(3): 514–515.
Publisher Full Text

43. Romeo E, Royo C, Monzón A: **Improved Explicit Equations for Estimation**

of the Friction Factor in Rough and Smooth Pipes. *Chem Eng J.* 2002; **86**(3): 369–374.
Publisher Full Text

44. Myhre G, Shindell D, Breon FM, *et al.*: **IPCC 2013 Assessment Report 5th Climate Change: The Physical Science Basis, the Intergovernmental Panel on Climate Change.** Cambridge University Press, Cambridge, United Kingdom and New York, NY, USA. (Chapter 8 Anthropogenic and Natural Radiative Forcing). 2013.

45. He Y, Cao F, Jin L, *et al.*: **Experimental Study on the Performance of a Vapor Injection High Temperature Heat Pump.** *Int J Refrig.* 2015; **60**: 1–8.
Publisher Full Text

46. Akau RL, Schoenhals RJ: **The Second Law Efficiency of a Heat Pump System.** *Energy.* 1980; **5**(8–9): 853–863.
Publisher Full Text

47. Taylor BN, Kuyatt CE: **Guidelines for Evaluating and Expressing the Uncertainty of NIST Measurement Results.** (Gaithersburg, MD: National Institute of Standards and Technology) NIST Technical Note 1297. 1994.
Reference Source

48. Bell IH, Lemort V, Groll EA, *et al.*: **Liquid Flooded Compression and Expansion in Scroll Machines - Part II: Experimental Testing and Model Validation.** *Int J Refrig.* 2012; **35**(7): 1890–1900.
Publisher Full Text

49. Siva Reddy V, Panwar NL, Kaushik SC: **Exergetic Analysis of a Vapour Compression Refrigeration System with R134a, R143a, R152a, R404A, R407C, R410A, R502 and R507A.** *Clean Techn Environ Policy.* 2012; **14**: 47–53.
Publisher Full Text

50. Meramveliotakis G, Kosmadakis G, Karellas S: **Test and numerical data of a vapour-injection scroll compressor in a heat pump with R1234ze(E) (Version 01) [Data set].** *Zenodo.* 2021.
http://www.doi.org/10.5281/zenodo.5785939

Open Peer Review

Current Peer Review Status: ✔ ✔

Version 2

Reviewer Report 07 December 2022

https://doi.org/10.21956/openreseurope.16569.r30425

© **2022 Wieland C.** This is an open access peer review report distributed under the terms of the Creative Commons Attribution License, which permits unrestricted use, distribution, and reproduction in any medium, provided the original work is properly cited.

✔

Christoph Wieland
Chair of Energy Systems, School, Technical University of Munich, Garching, Germany

My comments have been perfectly addressed. Thank you very much!

Competing Interests: No competing interests were disclosed.

Reviewer Expertise: Organic Rankine cycle power systems with expertise in both, experimental and numerical.

I confirm that I have read this submission and believe that I have an appropriate level of expertise to confirm that it is of an acceptable scientific standard.

Version 1

Reviewer Report 23 August 2022

https://doi.org/10.21956/openreseurope.15834.r29493

© **2022 Wieland C.** This is an open access peer review report distributed under the terms of the Creative Commons Attribution License, which permits unrestricted use, distribution, and reproduction in any medium, provided the original work is properly cited.

?

Christoph Wieland
[1] Chair of Energy Systems, School, Technical University of Munich, Garching, Germany
[2] Chair of Energy Systems, School, Technical University of Munich, Garching, Germany

A scroll compressor designed for R407C has been investigated for R1234ze(E). The main feature of the comppressor is its capability of vapor injection in between the compression process. This

increases the efficiency by reducing the compressor power. A simulation model is adapted and parametrized by the experimental data. Based on this model the performance is evaluated.

The open access of the operational data is much appreciated, as well as the indication of the sensor specifications of type and uncertainty. This allows a very good reproducibility of the results.

In terms of statistical evaluation of the data, the parity plots are very good and helpful. Some performance indicators might be helpful to compare especially the obtained improvements with the improved correlation.

In general, the publication is very well written and structured. In order to improve the quality of the paper even further, I recommend addressing the following comments:

1. Some minor typos and wordings should be corrected by a final proofreading (i.e. relative literature -> related literature, cubed exponent -> inverse cubed exponent, heat pumps systems -> heat pump systems, liluratre -> literature, regulation -> control, Wwhere -> Where, chocking valve -> choking valve, ...)

2. The quality and resolution of some of the figures need to be improved.

3. Is there any benefit in introducing weighting factors in the minimization function (equation 1)?

4. The authors note that data from the manufacturer and from experiments have been made. Is there any differentiation made between the two data sets? Or have they been merged? Has a separate analysis been performed?

5. Caption of Figure 1: To be more precise, please introduce dS=0 isentropic as well as dV=0 isochoric.

6. For the isentropic efficiency, I recommend to use \eta instead of n_is (page 6).

7. Please comment on the “best-fit procedure”. Out of which different correlations has been chosen?

8. Figure 3 could be displayed in log-formatted y-axis to allow for a better differentiation.

9. For the temperature ranges of the test conditions on page 10: Please indicate the temperature steps, if possible.

10. The authors write: “The heat pump was operating many hours per day”, but what was determining the operation: Experiments or daily ambient temperature? Maybe the authors can add a short explanation.

11. It is not clear how the authors determined steady-state for the operational points. It would be good to add a short explanation.

12. Is the compressor/heat pump cycle operated with pure working fluid or has a lubrication oil been added?

13. In the uncertainty analysis a standard reference on error propagation can be added.

14. Tables 5-6: Please harmonize the accuracy of parameter and uncertainty in terms of digits.

15. Fig. 7-9: Why is there no operational point at T_ev,in=10 °C and T_w,cond,out=35 °C?

16. With respect to the results section: A direct comparison between the two fluids would be helpful to facilitate the discussion of the results.

17. More importantly, I am missing a comparison of the working fluid and its thermo-physical parameters (i.e. supported by T-s-diagram). This will facilitate the explanations in the deviations of pressure drop and performance between the two fluids.

Is the work clearly and accurately presented and does it cite the current literature?
Yes

Is the study design appropriate and does the work have academic merit?
Yes

Are sufficient details of methods and analysis provided to allow replication by others?
Yes

If applicable, is the statistical analysis and its interpretation appropriate?
Partly

Are all the source data underlying the results available to ensure full reproducibility?
Yes

Are the conclusions drawn adequately supported by the results?
Yes

Competing Interests: No competing interests were disclosed.

Reviewer Expertise: Organic Rankine cycle power systems with expertise in both, experimental and numerical.

I confirm that I have read this submission and believe that I have an appropriate level of expertise to confirm that it is of an acceptable scientific standard, however I have significant reservations, as outlined above.

Author Response 10 Nov 2022

George Kosmadakis

Reviewer: A scroll compressor designed for R407C has been investigated for R1234ze(E). The main feature of the compressor is its capability of vapor injection in between the

compression process. This increases the efficiency by reducing the compressor power. A simulation model is adapted and parametrized by the experimental data. Based on this model the performance is evaluated.

The open access of the operational data is much appreciated, as well as the indication of the sensor specifications of type and uncertainty. This allows a very good reproducibility of the results.

***Authors**: We would like to thank the Reviewer for his comments. His suggestions, time and effort to review this work are really appreciated.*

In terms of statistical evaluation of the data, the parity plots are very good and helpful. Some performance indicators might be helpful to compare especially the obtained improvements with the improved correlation.

***Authors**: In order to compare the improved semi empirical model with the standard one, Table 9 includes some performance indicators concerning minimum, maximum and average deviation of the predicted variables with R407C refrigerant. A similar comparison is included in Table 11 for R1234ze(E).*

Reviewer: In general, the publication is very well written and structured. In order to improve the quality of the paper even further, I recommend addressing the following comments: Some minor typos and wordings should be corrected by a final proofreading (i.e. relative literature -> related literature, cubed exponent -> inverse cubed exponent, heat pumps systems -> heat pump systems, liluratre -> literature, regulation -> control, Wwhere -> Where, chocking valve -> choking valve...)

***Authors**: Thank you for your comments. All the typographical errors and wordings have been corrected.*

Reviewer: The quality and resolution of some of the figures need to be improved.

***Authors**: All the figures will be uploaded again with >= 300 dpi resolution.*

Is there any benefit in introducing weighting factors in the minimization function (equation 1)?

***Authors**: According to the literature, compressor or expander semi-empirical models are usually calibrated with no weighting factor in the minimization function, in order to favor evenly each factor (Temperature, mass flow rate and electricity). This has been also followed here.*

Reviewer: The authors note that data from the manufacturer and from experiments have been made. Is there any differentiation made between the two data sets? Or have they been merged? Has a separate analysis been performed?

***Authors**: The compressor data with R407C are extracted from the manufacturer selection software. These data then have been used, in order to calibrate the semi empirical model and to*

compare the outputs of the model with the manufacturer's results for validation reasons. The other data set was a separate one, and was obtained from the actual testing of the heat pump unit at the lab with the same compressor as for R407C but with R1234ze(E) refrigerant. These two datasets were analyzed and processed separately but they have been used as inputs to the same semi-empirical model.

Reviewer: Caption of Figure 1: To be more precise, please introduce dS=0 isentropic as well as dV=0 isochoric.

***Authors**: The suggested changes have been made.*

Reviewer: For the isentropic efficiency, I recommend to use \eta instead of n_is (page 6).

***Authors**: The symbol has been corrected.*

Reviewer: Please comment on the "best-fit procedure". Out of which different correlations has been chosen?

***Authors**: The fitting has been made based on the Zigrang & Sylvester correlation. This is now commented in the text as well.*

Reviewer: Figure 3 could be displayed in log-formatted y-axis to allow for a better differentiation.

***Authors**: The x axis of Figure 4 (Previous Figure 3) has been formatted to logarithmic in order for the trend to be more "linear". Logarithmic form of the y axis brings a minor improvement.*

Reviewer: For the temperature ranges of the test conditions on page 10: Please indicate the temperature steps, if possible.

***Authors**: The temperature steps (setpoints) at the evaporator were three (10, 15 and 25 ^{o}C). At each setpoint in the evaporator, the heat pump operated to heat up a large tank, with the condenser temperature started from about 30 ^{o}C and gradually reached 50 ^{o}C.*

Reviewer: The authors write: "The heat pump was operating many hours per day", but what was determining the operation: Experiments or daily ambient temperature? Maybe the authors can add a short explanation.

***Authors**: The operation was only for experimental reasons. The evaporator and condenser water side were connected to two large tanks. The "cold" tank at the evaporator side was equipped with electric resistances while the one at the condenser with an air source heat pump. Therefore, the temperature could be controlled in both tanks. This is included in the text just before the new Fig. 6.*

Reviewer: It is not clear how the authors determined steady-state for the operational points. It would be good to add a short explanation.

***Authors**: For the operational points and the final data set obtained from the measurements, 10-minute averaged values are selected from different working conditions. A short explanation has been added just before the new Table 5.*

Reviewer: Is the compressor/heat pump cycle operated with pure working fluid or has a lubrication oil been added?

***Authors**: The compressor is hermetic with an internal oil lubrication system which is achieved by pumping the oil through a haft from a sump located at the bottom part of the compressor. There is no additional (external) lubrication.*

Reviewer: In the uncertainty analysis a standard reference on error propagation can be added.

***Authors**: A standard reference has been added: Taylor B N and Kuyatt C E 1994 Guidelines for Evaluating and Expressing the Uncertainty of NIST Measurement Results (Gaithersburg, MD: National Institute of Standards and Technology) NIST Technical Note 1297.*

Reviewer: Tables 5-6: Please harmonize the accuracy of parameter and uncertainty in terms of digits.

***Authors**: Done.*

Reviewer: Fig. 7-9: Why is there no operational point at T_ev,in=10 °C and T_w,cond,out=35 °C?

***Authors**: Unfortunately, there were no available experimental data sets for this combination of temperatures.*

Reviewer: With respect to the results section: A direct comparison between the two fluids would be helpful to facilitate the discussion of the results.

***Authors**: A comparison between the two fluids has been added regarding the performance parameters with the two refrigerants in the results section.*

Reviewer: More importantly, I am missing a comparison of the working fluid and its thermo-physical parameters (i.e. supported by T-s-diagram). This will facilitate the explanations in the deviations of pressure drop and performance between the two fluids.

***Authors**: We would like to thank the reviewer for pointing this out. A comparison between the two fluids in terms of thermo-physical properties has been added in the testing facilities section.*

Competing Interests: No competing interests were disclosed.

Reviewer Report 08 July 2022

https://doi.org/10.21956/openreseurope.15834.r29592

© **2022 Tauveron N.** This is an open access peer review report distributed under the terms of the Creative Commons Attribution License, which permits unrestricted use, distribution, and reproduction in any medium, provided the original work is properly cited.

Nicolas Tauveron
[1] CEA, Liten, Univ., Grenoble Alpes University, Le Bourget du Lac, France
[2] CEA, Liten, Univ., Grenoble Alpes University, Le Bourget du Lac, France

The article deals with a very interesting subject: an improved heat-pump, including new "clean" (GWP<10) fluid. The paper concentrates on one of the main component of such system: the compressor. The compressor is of scroll technology. The scientific contribution is rather complete, involving experimental data and numerical model.
From a general point of view, the paper is clear, well-written and easy to follow.

The introductory part offers an interesting presentation of the context. However, I suggest that the auhtors include a precise definition of high-temperature heat pump (HTHP) and low GWP refrigerant. Moreover, some additional elements concerning lubrication and oil could be useful in the presentation.

The second part is devoted to the model presentation and is generally clear, except the Wcp definition. It is not clear to me if this value includes mechanical and electrical conversion or not.

Next section concerns the experimental test rig. The fact that the design fluid was R407C (and not R1234zd(E)) could be commented through a table or a P-h diagram. The facility is well described, but a general thermodynamic diagram in complement to Figure 5 could help the reader. Specific comments about the use of two types of expansion valve could be interesting.

Next step concerns cycle analysis. We suppose that heat losses were not considered during cycle analysis (excepting in the compressor); perhaps we miss it, otherwise this could be clarified.

Next section concerns a technical discussion on the results. Two main technical elements are underlined and discussed. The first concerns the question of pressure losses increase in the case of using R1234zd(E). The technical reasons are well identified: a decrease of Re leading to quasi-laminar regime. The authors investigate more accurate correlations & models to take into account flow regime modification. These elements are clear and convincing. Perhaps the authors could suggest some geometrical modifications to increase fluid velocity or turbulence.

The second concerns "compressor losses" and is, to my opinion, the most debatable part of the work. We clearly understand that the models are used to determine parameters (Table 7 for R407C and Table 9 for R1234zd(E)). Compressor losses increase is coherent with the parameters found. However, it is really surprising that some parameters are highly modified, such as the different AU, "constant terms for losses", etc ... values between the two fluid cases. I suggest that the authors could explain the main modifications due to fluid properties as they did for pressure losses modification. An example concerns AUam value modification from 12 to 1600: A(=area) should not vary a lot, and U can certainly vary a lot due to regime modification and consequently Nusselt value. A short analysis of Nusselt correlations could help the reader to understand some

effects. The other example concerns the 'constant term' of electrical pressure losses: could the authors indicate why this 'constant' varies between the two configurations (276->490). I would suggest, but I do not know if it is really possible, that the approach could alternatively consider some parameters kept constant between the two configurations and the others would vary. Such an approach could help to give more predictive (and not only descriptive) results.

The conclusion is clear, honest and really useful for the reader as the different points of the work are presented. I have appreciated that they are quite nuanced.

Is the work clearly and accurately presented and does it cite the current literature?
Yes

Is the study design appropriate and does the work have academic merit?
Yes

Are sufficient details of methods and analysis provided to allow replication by others?
Yes

If applicable, is the statistical analysis and its interpretation appropriate?
Yes

Are all the source data underlying the results available to ensure full reproducibility?
Yes

Are the conclusions drawn adequately supported by the results?
Yes

Competing Interests: No competing interests were disclosed.

Reviewer Expertise: Applied thermodynamic

I confirm that I have read this submission and believe that I have an appropriate level of expertise to confirm that it is of an acceptable scientific standard.

Author Response 10 Nov 2022

George Kosmadakis

Reviewer: The article deals with a very interesting subject: an improved heat-pump, including new "clean" (GWP<10) fluid. The paper concentrates on one of the main component of such system: the compressor. The compressor is of scroll technology. The scientific contribution is rather complete, involving experimental data and numerical model. From a general point of view, the paper is clear, well-written and easy to follow.

Authors*: We would like to thank the Reviewer for his valuable comments which greatly help to improve this work.*

Reviewer: The introductory part offers an interesting presentation of the context. However, I suggest that the authors include a precise definition of high-temperature heat pump (HTHP) and low GWP refrigerant. Moreover, some additional elements concerning lubrication and oil could be useful in the presentation.

***Authors**: A more precise definition according to literature has been added in the introduction for both low GWP refrigerants and HTHPs according to their typical operating temperatures. In addition, some comments have been provided concerning the increase of oil performance when a compressor with an economizer port is preferred (due to the lower temperatures).*

Reviewer: The second part is devoted to the model presentation and is generally clear, except the Wcp definition. It is not clear to me if this value includes mechanical and electrical conversion or not.

***Authors**: The compressor electrical power Wcp* $\dot{W}_{cp}$ *includes electromechanical conversion and all related losses. To make this clearer, its definition has been enriched just after Eq. (7) in the revised text.*

Reviewer: Next section concerns the experimental test rig. The fact that the design fluid was R407C (and not R1234zd(E)) could be commented through a table or a P-h diagram. The facility is well described, but a general thermodynamic diagram in complement to Figure 5 could help the reader. Specific comments about the use of two types of expansion valve could be interesting.

***Authors**: The two refrigerants R407C and R1234ze(E) are now compared in a new section, including a table with their thermo-physical properties (new Table 3) and a figure with the compressor envelope for each refrigerant. Additionally, some comments for the operation and control of the two expansion valves have been included. Furthermore, in Figure 6 (old figure 5) the P-H diagram of the thermodynamic cycle has been added.*

Reviewer: Next step concerns cycle analysis. We suppose that heat losses were not considered during cycle analysis (excepting in the compressor); perhaps we miss it, otherwise this could be clarified.

***Authors**: The heat losses at the pipes and the pressure drop have been included in the cycle analysis, in order to calculate the fluid properties at the inlet of each component (e.g. plate heat exchangers, compressor, expansion valve, etc.). A short explanatory comment has been added in the revised text in the Data reduction section (before Table 6) to make this clearer.*

Reviewer: Next section concerns a technical discussion on the results. Two main technical elements are underlined and discussed. The first concerns the question of pressure losses increase in the case of using R1234zd(E). The technical reasons are well identified: a decrease of Re leading to quasi-laminar regime. The authors investigate more accurate correlations & models to take into account flow regime modification. These elements are clear and convincing. Perhaps the authors could suggest some geometrical modifications to increase fluid velocity or turbulence.

***Authors**: The compressor is a commercial one and for that reason the suction port has a fixed geometry with a specific diameter. Therefore, no modifications could be applied, with the only option to replace the compressor with a compatible one with R1234ze(E), but without an economizer port.*

Reviewer: The second concerns "compressor losses" and is, to my opinion, the most debatable part of the work. We clearly understand that the models are used to determine parameters (Table 7 for R407C and Table 9 for R1234zd(E)). Compressor losses increase is coherent with the parameters found. However, it is really surprising that some parameters are highly modified, such as the different AU, "constant terms for losses", etc ... values between the two fluid cases. I suggest that the authors could explain the main modifications due to fluid properties as they did for pressure losses modification. An example concerns AUam value modification from 12 to 1600: A(=area) should not vary a lot, and U can certainly vary a lot due to regime modification and consequently Nusselt value. A short analysis of Nusselt correlations could help the reader to understand some effects. The other example concerns the 'constant term' of electrical pressure losses: could the authors indicate why this 'constant' varies between the two configurations (276->490). I would suggest, but I do not know if it is really possible, that the approach could alternatively consider some parameters kept constant between the two configurations and the others would vary. Such an approach could help to give more predictive (and not only descriptive) results.

***Authors**: The semi-empirical model which is developed and used includes the main losses but cannot predict all the phenomena especially when the compressor works near to the envelope limits. For example, AUamb is related to the shell temperature of the compressor. This high value in the case of R1234ze(E) has more mathematical than physical meaning and states that the shell temperature needs to be reduced so that it transfers more heat to the surroundings, in order to avoid heating up the refrigerant at the suction, trying to match with the experimental measurements. Due to the high pressure loss at the suction, the compression starts from lower temperature and ends to lower discharge temperature accordingly. To possibly resolve this un-physical values, the shell envelope could be split in two regions, one for the upper part (the hotter) and the other for the bottom (the colder), but in this case the complexity increases, because two shell temperatures need to be considered. This is to be evaluated in the future, whether it could contribute to the model accuracy. A short comment has been added in the revised text (2nd paragraph after new Table 10) to clarify this. Moreover, the parameters such as Vs,cp, K, acp, and $\dot{W}$loss,0 are expected not to vary for different fluids, since they don't depend on refrigerant properties. However, the semi-empirical model accuracy is enhanced when these parameters are recalculated during the calibration process for every refrigerant. This could be related to the assumptions of the model as well as the systematic and random errors of the data set used for the calibration.*

Reviewer: The conclusion is clear, honest and really useful for the reader as the different points of the work are presented. I have appreciated that they are quite nuanced.

***Authors**: We would like to thank you once again for your valuable comments, suggestions and your precious time spent in reviewing our manuscript.*

Competing Interests: No competing interests were disclosed.